Calorimetric study of carbon dioxide (CO2) hydrate formation and dissociation processes in porous media

Fatima Doria Benmesbah, Pascal Clain, Olivia Fandino, Véronique Osswald, Laurence Fournaison, Christophe Dicharry, Livio Ruffine, Anthony Delahaye

Calorimetric study of carbon dioxide (CO_2) hydrate formation and dissociation processes in porous media

Fatima Doria Benmesbah[a,b],* Pascal Clain[c, a*], Olivia Fandino[b], Veronique Osswald[a], Laurence Fournaison[a], Christophe Dicharry[d], Livio Ruffine[b], Anthony Delahaye[a]

[a] Université Paris-Saclay, INRAE, FRISE, 92761, Antony, France.

[b] IFREMER, Département Ressources physiques et Ecosystèmes de fond de Mer (REM), Unité des Géosciences Marines, 29280 Plouzané, France

[c] Leonard de Vinci Pôle Universitaire, Research Center, 12 avenue Léonard de Vinci, 92916, Paris La Défense, France

[d] CNRS/TOTALENERGIES/UNIV PAU & PAYS ADOUR, Laboratoire des Fluides Complexes et leurs Réservoirs - IPRA, UMR5150, 64000, Pau, France

*Corresponding author(s): Fatima Benmesbah: benmesbah.fatimadoria@gmail.com; Pascal Clain: pascal.clain@devinci.fr

Abstract

Understanding the formation and dissociation mechanisms of gas hydrate in porous media is important for the development of new energy-efficient and environmentally friendly technologies related to cold storage as they provide significant latent heat and energy density at suitable phase change temperature. The challenge is to understand the interactions between gas hydrates and the chosen storage media in order to assess the operating conditions likely to optimize time and energy consumption in cold production and storage systems. In this work, CO_2 hydrates formation and dissociation are investigated in two morphologically different porous materials: sand and silica gels. A calorimetric approach is applied to study both the CO_2 hydrate formation kinetics, particularly the induction time, and the amount of hydrate formed for each of the two porous materials. The experiments are performed using a

differential thermal analysis device with two identical measuring cells. The present work is focused on assessing the effect of key factors like water saturation, particle size and the morphology of porous media on CO_2 hydrate formation and dissociation processes. Overall, the results do not show a statistically significant correlation between these factors and the induction time. Interestingly, the results obtained with dual porous silica gel showed a higher amount of hydrate formed compared to those with sand for similar initial pressure, temperature and water content conditions. This result may be due to the fact that silica gels provide higher surface area due to their smaller particle size (20-45 µm vs. 80-450 µm for sand), and the presence of internal pore volume in silica gel particles.

Keywords: CO_2 hydrate, Cold storage, Differential thermal analysis, Particle and Pore size, Porous media, Water saturation

1. Introduction

Industry requirements for thermal energy production and storage are increasing to meet human needs, for example, for food conservation, refrigeration and air conditioning. However, cold production is responsible for 20 % of the electrical energy consumed in industrial countries and 8 % of greenhouse gas emissions due to traditional refrigeration processes. Indeed, these processes use harmful refrigerants such as Chlorofluorocarbons (CFCs) and Hydrochlorofluorocarbons (HCFCs) that are relevant to radiative forcing and stratospheric ozone depletion, but also, Hydrofluorocarbons (HFCs) which, like CO2, are linked only to radiative forcing. These coolants have a much higher global warming potential than carbon dioxide (for example, CFC-12, HCFC-22 and HFC-134a are respectively 10 900, 1 810 and 1 430 times as warming as carbon dioxide over a 100-year period (Forster and Venkatachalam, 2005). In an attempt to contain and reduce the use of these refrigerants, secondary refrigeration has been proposed as an interesting and promising solution. It introduces the use of environmentally neutral refrigerants that conduct thermal energy in a secondary circuit to the cooling point (Delahaye et al., 2018; Wang et al., 2015).

The development of a cost-effective and environmentally friendly secondary refrigeration system requires a good balance between energy demand and supply. In this context, the cooling capacity of the system has to be sufficient during peak hours when energy consumption is high. Cold storage is a suitable method to increase this cooling capacity. Indeed, cold storage devices can be used to store cold thermal energy during off-peak periods, and use it during peak hours, which contributes to peak shaving and refrigerating system downsizing. Hence, cold storage offers flexibility in energy consumption by ensuring spatial and temporal regulation. This is why most of the industrial achievements combine cold production and storage systems. Traditionally, cold storage technologies use ice, chilled water or eutectic salt (Akbari and Mertol, 1989; Cheng et al., 2020). However, some of these

storage media have low energy efficiency and can be very costly (Hasnain, 1998). The challenge of this technology is to select a refrigerant with high energy density and high heat transfer capacity in order to reduce the system power consumption. One of the solutions that is currently under consideration is the use of phase change materials for such a technology.

Among the phase change materials that have the most suitable criteria for the refrigeration industry, gas hydrates have attracted the attention of several researchers who considered them as a potential candidate, primarily due to their interesting thermodynamic properties (Sloan, 1998; Sloan and Fleyfel, 1992). Gas hydrates are non-stoichiometric crystalline structures composed of hydrogen-bonded water molecules forming cavities, generally called cages. These cavities can trap gas molecules like hydrogen, nitrogen, helium, methane, carbon dioxide or hydrocarbons and so on (Loveday and Nelmes, 2008; Sloan and Koh, 2007), which stabilizes the hydrate structure. Gas hydrates are stable under low temperature and high-pressure conditions. The attractive properties of gas hydrates include their high gas storage capacity, their increased gas selectiveness capacity and their high dissociation enthalpy. In addition, they are stable over a wide range of temperatures (in particular for T > 273 K, for example, CO_2 hydrates can form at a rough range of temperatures between 273 and 283 K, and an approximate pressure range of 1.5-4.5 MPa), which is of a particular interest for air conditioning (Englezos, 1993; Fournaison et al., 2004; Li et al., 2012).

The development of a CO_2 hydrate-based cold production, transport and storage system requires intensive studies on the kinetic, thermodynamic and rheological characteristics of CO_2 hydrate slurries (gas hydrate crystals suspended in water), which were the focuses of many studies in the past (Boufares et al., 2018; Darbouret et al., 2005; Delahaye et al., 2008; Dufour et al., 2017; Jerbi et al., 2010; Kumar et al., 2016; Prah and Yun, 2018; Shindo et al., 1993). Several of them pointed out a slow gas hydrate formation rate and a low storage density in bulk media (Englezos et al., 1987; Linga et al., 2010). In order to enhance energy

efficiency of hydrate-based industrial applications, several solutions that involve specific properties have been proposed such as acceleration of the formation process by stirring in order to improve gas mass transfer to liquid by enhancing the gas-liquid contact interface (Linga et al., 2012; Wang et al., 2014); the use of acoustic waves (Laugier et al., 2008; Wang and Dennis, 2017) or the use of kinetic or thermodynamic chemical additives (Joshi et al., 2013; Kang et al., 2001; Kumar et al., 2013; Martínez et al., 2008; Torré et al., 2011). According to a recent review of literature enhancing mass transfer by forming CO_2 hydrates in porous media could improve Cold Thermal Energy Storage (CTES) design (Wang et al., 2020). However, related current research is focused on other applications such as gas separation (Yang et al., 2015), CO_2 sequestration (Oya et al., 2017), and mainly on understanding natural hydrate dynamics (Malagar et al., 2019; Zhang et al., 2017). To our knowledge, very few studies have been published on the use of porous media in CO_2 hydrate-based cold storage technologies. Indeed Clain (2014) mentioned the interest and the kinetic and thermodynamic influence of porous media which can constitute a simple solution to implement for the development of a multi-temperature storage process from hydrates. More recently, Cheng et al. (2020) reported on the use of porous media as a hydrate reinforcement method aiming at reducing the induction time of hydrate formation, increasing nucleation rates, and bettering the cold storage density of the cold storage media. In addition, as mentioned previously Wang et al. (2020) pointed out in a review that one of the important challenges of CTES systems based on CO_2 hydrates is a low mass transfer due to limited gas-liquid interface. The authors suggested the use of porous media in future work to improve mass transfer and thus the gas-liquid interface.

In a series of investigation on gas hydrates formation and dissociation kinetics, it has been shown an improvement of gas hydrate formation as well as water to hydrate conversion rates in a packed bed of silica sand particles compared to a stirred vessel (bulk media) (Linga and

Clarke, 2017; Linga et al., 2009). Indeed, porous media offer a relatively large contact surface compared to bulk media. They allow a better distribution of the liquid and vapor phases by adsorption on the surface of the particles and with the help of capillary forces, thus increasing the gas-water contact. Therefore, the mechanisms of gas hydrate formation and dissociation in porous media must be carefully considered.

In order to provide a large surface area and potentially to limit energy consumption related to the stirring required in bulk media, the present paper seeks to address CO_2 hydrates formation and dissociation in porous media using a calorimetric approach. Several studies attempted to investigate the interaction between gas hydrates and the porous media in which they form (Adeyemo et al., 2010; Bagherzadeh et al., 2011; Chong et al., 2016; Fitzgerald et al., 2014; Ge et al., 2019; Heeschen et al., 2016; Kang et al., 2013; Kumar et al., 2015; Mekala et al., 2014; Nguyen et al., 2020; Qin et al., 2022; Smith et al., 2002; Wang et al., 2021; Zhang et al., 2022; Zhang et al., 2016). This literature draws attention to the effect of several factors on gas hydrate formation rate and water to hydrate conversion, such as:

(1) The nature of porous media (surface chemistry, morphology: pore and particle size). Indeed, for particle size, a number of studies demonstrated an increase in the amount of hydrates formed, with higher gas consumption by hydrates and/or higher water-to-hydrate conversion rate for smaller particle sizes tested (Bhattacharjee et al., 2015; Ge et al., 2019; Mekala et al., 2014). For example, Ge et al. (2019) performed CH_4 hydrate formation in a high-pressure reactor using two particle size classes of silica sand, 180-250 and 300-900 µm. The porous media was 70 % saturated with pure water. The authors demonstrated higher gas consumption by hydrates and water-to-hydrate conversion for the smallest particle size. This tendency is also observed for smaller pore sizes (Zhang et al., 2015). However, other studies demonstrated an opposite result concerning the influence of particle size (Adeyemo, 2008; Kumar et al., 2015; Lu et al., 2011; Pan et al., 2018). In fact, Pan et al. (2018) performed CH_4

hydrate formation in silica sand for various particle sizes, 38, 48, 74, 106 and 165 µm. In their study, they used a 300-ppm (mass fraction) of sodium dodecyl sulfate (SDS) solution for all experiments with a liquid phase saturation of 50 %. The results showed that gas storage capacity and water to hydrate conversion rate increase with the increase of particle size (0.101 mol of gas/mol of liquid and 61.9 % water to hydrate conversion rate for 38 µm particle size, versus 0.151 mol of gas/mol of liquid and 92.2 % water to hydrate conversion rate for 165 µm particle size). The authors suggested that smaller particle sizes lead to narrow pores, which can decrease connectivity of the porous media, and slower CH_4 diffusion in the liquid phase. Globally, it has been suggested that hydrates formed in smaller pores may obstruct gas diffusion in the porous media.

(2) The operating conditions (pressure, temperature, water saturation, gas solubility, etc.). Indeed, several studies have shown that water saturation affects not only the final hydrate saturation, but also the gas transport within the porous medium (Babu et al., 2013; Bagherzadeh et al., 2011; Ge et al., 2019; Kumar et al., 2015). Some of these studies have shown that at low water saturation, gas transport in the pore medium is facilitated, and liquid-gas contact is improved. As a consequence, the formation of hydrates is also improved. However, some authors have shown that low water saturation limits the amount of water available for hydrate formation (Babu et al., 2013; Kumar et al., 2015). Based on the above studies, it is noted that water saturation is an important factor that requires further and extensive studies to determine the optimal water saturation conditions for gas hydrate formation in the studied porous media.

Obviously, the effects of porous structure on gas hydrates formation kinetics, particularly on induction time, are not fully understood, as well as, the effect of the nature of porous media on gas-liquid contact area and on heat/mass transfer.

To better control gas hydrates formation and dissociation in a cold storage system, it is of great interest to study CO_2 hydrate formation kinetics and their thermodynamic stability conditions, as well as the possible energy storage of the porous media containing CO_2 hydrates. The present paper aims to provide further insight into CO_2 hydrate formation and dissociation processes in porous media based on heat and mass transfer characterization. Using a differential thermal analysis method, an original approach in literature to study CO_2 hydrates in porous media for cold storage purpose, the effect of key factors such as water saturation, particle size and the morphology of the porous media on the solid mass fraction formed was investigated. For the latter, two morphologically different porous media were used: silica sand and dual porous silica gel. The experimental data obtained add to a growing body of literature on the influence of porous media on gas hydrate formation and dissociation processes, in an attempt to enhance energy efficiency of industrial applications such as hydrate-based cold storage systems.

2. Experimental section

CO_2 hydrates formation and dissociation experiments were conducted using differential thermal analysis, which is an accurate and suitable method of characterizing thermal properties such as dissociation enthalpy of gas hydrates. This heat-flux calorimetry method is traditionally used to measure various thermo-physical properties of gas hydrates (Gupta et al., 2008; Kang et al., 2001; Lievois et al., 1990). The principle is based on the use of two identical cells connected to each other by several thermocouples. This connection allows an instantaneous and precise measurement of the temperature change between the two cells when a phase change occurs in one of the cells. A detailed description of the method is given in the following subsections.

2.1.Materials

Carbon dioxide with a certified purity of more than 99.7 % was supplied by Linde Gas (France). Fontainebleau silica sand purchased from Laboratoires Humeau (La Chapelle-sur-Erdre, France) and spherical silica porous gel particles of nominal pore diameters of 30 and 100 nm supplied by Silicycle Co. (Canada) were used as porous media. All materials were used without further purification. The detailed properties of silica sand and silica gel are listed in Table 1.

Table 1: Physical properties of Fontainebleau silica sand and silica gel samples.

Parameters	**Fontainebleau silica sand**	**30 nm Silica gel**	**100 nm Silica gel**
Mean particle diameter (µm)	80-450	20-45	20-45
Mean pore diameter (nm)	-	30	100
Pore volume ($cm^3.g^{-1}$)	-	0.86	0.7
Dry density ($g.cm^{-3}$)	2.65	2.2	2.2

To study the influence of particle size on CO_2 hydrate formation and dissociation, Fontainebleau silica sand was sieved to 3 classes of particles: 80 to 160 µm; 160 to 315 µm and 315 to 450 µm noted respectively PS01, PS02 and PS03.

2.2.Differential thermal analysis (DTA) apparatus description

A differential thermal analysis (DTA) apparatus was used for the experiments, whose principle was described in a previous work (Fournaison et al., 2004). It was designed to measure the difference in thermal behavior between two identical cells submitted to the same heat flux. A schematic diagram of the experimental apparatus is shown in Figure 1. It consists of two identical and symmetric transparent glass cells with a functional volume of 40 ml. The transparent walls enable visualization of the studied samples inside the cells.

The two cells are immersed in a temperature-controlled bath (blue area in Figure 1). One of them is filled with the porous media at a certain water saturation and used as the reactor for hydrate formation (called measurement cell). The second cell (called reference cell) is filled with the same porous media and water saturation as the measurement cell with an inert solution of water-ethanol 50 % vol/vol, in order to avoid crystallization during the thermal cycle while having thermal properties close to those of the liquid in the measurement cell. The measurement cell is connected to a CO_2 supply line, which contains a cylinder with a volume of 10 cm^3 (±10 % tolerance on the volume) and three manual valves to allow gas supply. The cylinder is also immersed in the temperature-controlled bath. It allows (1) to determine the amount of gas injected in the measurement cell and (2) to limit the risk of overpressure in the glass cell. Indeed, CO_2 is injected in the measurement cell using a successive gas expansion method. This method consists of injecting the gas into the sample cylinder while keeping valve 1 closed. Valve 3 is then closed to disconnect the gas supply. Once the pressure in this circuit is stable, valve 1 is open to allow gas expansion in the cell. This operation is repeated several times until the targeted experimental pressure around 2.5 MPa is reached. The amount of CO_2 injected (mole) in each operation is calculated by the difference between the amount of CO_2 (mole) present in the circuit (between valve 1 and valve 3) before and after expansion to the cell.

The pressure is measured at two points: the first pressure sensor (0-10 MPa. 0.011 % full scale. Keller) is located at the inlet of the measuring cell, and a second one (0-10 MPa. 0.006 % full scale. Keller) at the inlet of the gas supply line.

Each cell is equipped with one thermocouple that gives a direct temperature measurement (±0.5 K). The DTA measurement is based on the use of six thermocouples, three of which are inserted in one cell and three in the other. All thermocouples are located at the lowest part of the cell. These six thermocouples are connected together in series, by a back and forth connection between the two cells, as shown in Figure 2. This connection makes it possible to obtain an electrical signal directly linked to the difference in temperature between the two cells, and consequently to the difference in heat flow, knowing that the two cells are immersed in the same temperature-controlled bath.

The first advantage of this direct connection between the two cells is to allow an "instantaneous" measurement of the temperature difference, and not a difference between two temperature values measured by two individual thermocouples (which would each imply a measurement error). Another interest of the back and forth connection is to amplify the differential signal between the two cells, while limiting the error to one measurement, i.e. the signal recovered by the acquisition unit. This avoids the cumulative errors that could be obtained if six thermocouples were used individually.

2.3.Experimental procedure

2.3.1. Sample preparation and characterization

Silica sand samples at various water saturation were prepared using the following procedure: first, silica sand was dried at 388.15 K for 24 h. Then an amount of water corresponding to the desired water saturation was added to the sand at ambient temperature. The porosity of the unpacked sand was estimated by the supplier (Humeau Laboratories) to be approximately 0.44. Finally, the mixture was introduced into the measurement cell and packed evenly to fill

245 the entire volume. In order to evaluate the water distribution in the sand samples, an X-ray
246 micro-tomography experiment (DeskTom 130®, RX Solution, Chavanod, France) was
247 performed on a sand sample with 66 % water saturation. The sample was prepared under the
248 same conditions as the hydrate formation experiments, but in a transparent resin cell
249 (Formlabs, Clear PhotoPolymer) which has the same internal volume as the DTA cells (inner
250 diameter = 3 cm, height = 6.4 cm). This sample was then placed in the micro-tomography
251 device.

252 The analysis was performed with a voltage of 124 µV and a voxel size of 27.33 µm. XAct 2®
253 software (RX Solution, Chavanod, France) was then used for 3D-reconstruction from raw
254 images. A 3D-visualization and volume fractions of the phases within the sample (sand, water
255 and air) were obtained using Avizo 2019.1® software (Thermo Fisher Scientific, Waltham,
256 USA). Figure 3 shows the images obtained after the 3D-reconstruction. Due to the size of the
257 sample, which produces a very large data file, the image processing was performed on two
258 volumes (clipped) located in the upper and lower part of the sample. The idea was to have a
259 clearer view on the water distribution over the sample. The latter contains three phases; sand
260 (represented in yellow), water (blue) and air (dark grey). Table 2 shows information about the
261 volume fractions of the different compounds contained in the selected parts.

262 Table 2: Volume fractions of air, water and packed silica sand within the analyzed volumes
263 by micro-tomography

Analyzed Volume	Material	Volume fraction (%)	Total volume (cm^3)
Upper part	Air	0.10	0.529
	Water	0.19	
	Silica Sand	0.71	
Lower part	Air	0.10	0.190
	Water	0.19	
	Silica Sand	0.71	

Overall, based on Figure 3 and Table 2 analysis, it can thus be reasonably assumed that the filling method used for silica sand samples leads to a homogeneous water dispersion in the porous media since the same distribution of the various compounds was observed by micro-tomography at different spatial positions of the sample.

In order to address the limitations related to the mass transfer of gas, and water-gas contact in the porous media, and in light with previous studies (Adeyemo, 2008; Adeyemo et al., 2010; Dicharry et al., 2013; Kang et al., 2008; Kumar et al., 2013; Park et al., 2006), it seems to be important to study media with different morphologies (presence or not of dual porosity), in order to enhance the amount of energy stored per volume. In fact, dual porosity media may present two advantages for cold storage system:

1) Provide an additional internal surface area,

2) Provide a better diffusion of gas through the porous media, since water can occupy the internal pore volume thanks to capillary forces, thus leaving the interstitial space potentially free for gas diffusion (as represented by the schematic illustration in Figure 4).

Silica gel samples were prepared using a procedure from Dicharry et al. (2013). The procedure consists of layering uniformly the dried silica gel and water at 393.15 K for 24 h in various stages alternatively. The amount of water introduced at each layer is identical to the desired saturation of the pore volume of silica gel. The same procedures (for sand or silica gel) were used to fill the reference cell. Finally, the measurement cell was closed and residual air was removed with a vacuum pump.

2.3.2. DTA analysis of CO_2 hydrate formation and dissociation in silica sand

After pressurizing the measurement cell with CO_2 using an expansion method to the desired experimental pressure set around 2.5 MPa, the bath temperature was then set to 285.15 K to

288 stabilize the temperature inside both cells at an initial equilibrium state. Figure 5 shows the
289 evolution of pressure, temperature and DTA signal during an experiment in sand initially
290 saturated with water at 33 %. After the initial equilibrium state, the system was gradually
291 cooled down until 271.15 K.

292 The temperature peak (red line) indicates CO_2 hydrate formation due to the exothermic
293 property of crystallization. Meanwhile, the DTA signal peak (blue line) illustrates the
294 difference in heat transfer between the two cells. Thus, when the temperature conditions are
295 close in both cells, the DTA signal is close to zero. However, when the exothermic reaction
296 occurs in the measurement cell, the DTA signal increases rapidly with a similar pattern
297 compared to the direct measurement of the temperature. CO_2 hydrate formation is also
298 accompanied with a temperature peak and a strong decrease in the system pressure due to the
299 consumption of CO_2 during the hydrate growth. Figure 5b shows the presence of two
300 consecutive DTA peaks (2 red arrows on Figure 5b). These two peaks are accompanied with 2
301 consecutive pressure drops corresponding to gas consumption by hydrates. This result
302 suggests the occurrence of multiple nucleation followed by growth of CO_2 hydrates in silica
303 sand. This behavior occurred for all experiments within silica sand. When pressure,
304 temperature and DTA signal stabilized the thermodynamic equilibrium was considered to be
305 reached, and CO_2 hydrate formation finished. Hydrate dissociation was triggered by
306 increasing the bath temperature gradually with a rate of 0.1 $K.min^{-1}$ until the initial
307 temperature was reached (285.15 K). As shown in Figure 5a and c, hydrate dissociation is
308 expressed by a large and opposite variation in the DTA signal compared to hydrate formation.
309 This is due to the endothermic nature of hydrate dissociation. The temperature condition was
310 then maintained at 285.15 K to ensure a complete hydrate dissociation. Due to supercooling
311 phenomena related to the crystallization of gas hydrates, the exploitation of the DTA signal
312 peak related to hydrate formation remains difficult. Indeed, the formation being done by

breakage of supercooling, in bulk, and with high driving force, in porous media, the formation peaks quality strongly depends on the operating conditions. For this reason, dissociation peaks are generally used in calorimetry work (Chami et al., 2021; Lin et al., 2014). Thus, the discretization of the DTA signal obtained during hydrate dissociation was performed to determine the experimental dissociation enthalpy and calculate the mass of hydrates formed in the reactor.

2.3.3. Effect of the pore size of silica gel on equilibrium conditions of CO_2 hydrates

The effect of dual porous silica gel on the thermodynamic conditions of hydrate stability was examined. Figure 6a presents the results related to dissociation temperature of CO_2 hydrates in silica gel with a pore volume of 100 nm and 30 nm. These results are plotted in a P-T diagram and compared to the bulk-CO_2 equilibrium curve. A shift can be seen between the bulk-CO_2 hydrate equilibrium curve and that obtained in silica gel with a nominal pore size of 100 nm and 30 nm. For instance, with a pressure of 1.46 MPa, the two equilibrium temperatures present a shift of 0.7 K towards lower temperature conditions in comparison with the bulk equilibrium curve. Figure 6b shows that these results are consistent with those reported in the literature using several pore sizes of silica gel. All three-phase equilibrium points of CO_2 hydrates in silica gel with varying nominal pore sizes show a deviation from the bulk equilibrium curve of CO_2 hydrates. In addition, a decrease in pore size (going from 100 to 30 and then to 15 nm) resulted in a higher shift from the CO_2 hydrate equilibrium curve. In general, the presence of mesoporous volume from the ten to fifty nanometer scale generates an inhibiting effect for the formation of hydrates in silica gel. This can be explained by an important capillary effect generated by small pore size. Indeed, water being confined in very small pore size leads to a high capillary pressure. Consequently, the system needs more energy in order to overcome these forces and form hydrates in the mesoporous volume. This result is also demonstrated in several previous studies for CO_2, CH_4 and C_3H_8 (Adeyemo et

al., 2010; Babu et al., 2013; Dicharry et al., 2013; Handa and Stupin, 1992; Smith et al., 2002; Turner et al., 2005; Uchida et al., 2002; Yang et al., 2012).

2.3.4. Calibration and quantification of the amount of CO_2 hydrates formed

It is important to mention that the DTA technique is based on the determination of relative properties that depend on the heat transfer between the bath and the measurement/reference cell, which is related to the system configuration and geometry. Therefore, a calibration experiment consisting of formation and dissociation procedure applied to a calibration material with known properties is required for each new configuration (the geometric characteristics, nature of the porous media, water saturation, etc.). In this case, the calibration material is ice since its thermal properties are well known. This calibration experiment is based on the same procedure as for hydrate formation but without the gas injection step. The integration of the DTA peak during ice melting is used to determine a calibration coefficient C_{ice}. This coefficient is used to calculate the amount of energy consumed by hydrate dissociation as follows:

$$E_{exp}(kJ) = \left| C_{ice} * A_{hyd} \right| \quad (1)$$

A_{hyd} represents the result of the integration of the DTA signal peak related to hydrate dissociation. The mass of hydrates formed is computed using the experimental enthalpy obtained by equation (1) and the theoretical enthalpy of gas hydrates ΔH_{hyd} known to be equal to 500 kJ/kg_{water} (374 $kJ/kg_{hydrates}$) (Anderson, 2003; Fournaison et al., 2004):

$$m_{hyd}(kg) = \frac{E_{exp}}{\Delta H_{hyd}} \quad (2)$$

This equation does not take into account the variation over time of the difference in sensible heat between the two cells. This variation only implies an error of approximately 2% on the total amount of heat exchanged.

Water to hydrate conversion rate is computed from the following equation:

$$C_{wh}\ (\%) = \frac{m_{hyd} * n_h * M_{H_2O}}{\rho_{hyd} * m_{H_2O}} * 100 \qquad (3)$$

Hydration number n_h used for the present study is 7.23 (Kang et al., 2001), ρ_{hyd} is the density of CO_2 hydrate computed using the previous hydration number and m_{H_2O} is the mass of water introduced initially in the porous media.

3. Results and discussion

The efficiency of cold storage system using gas hydrates is related not only to thermodynamic equilibrium conditions, but also to gas hydrates formation and dissociation kinetics, and ultimately to the amount of cold thermal energy that can be stored and released per volume unit. In this study, the DTA apparatus described in the previous section was used to investigate particularly the effect of key factors related to the geometric characteristics of porous media and the operating conditions (water saturation, particle size and the morphology of the porous media) on the following storage properties:

1) The mass of CO_2 hydrates formed in the porous media determined by measuring the heat consumed during gas hydrate dissociation. It is of importance to identify the factors that influence the amount of hydrate formed, and thus, the amount of energy available in a cold storage system.
2) The induction time where no significant macroscopic changes are observed. It corresponds to the period between the moment when the system reaches the CO_2 hydrates bulk Hydrate-Liquid-Vapor equilibrium conditions (Sloan and Koh, 2007) (which are considered as reference equilibrium conditions) and the moment when a rapid hydrate crystal growth is detected. The induction time is a significant index when studying hydrate growth kinetics. It is well known in the literature that induction time measurements can be relatively difficult due to the stochastic nature of hydrate

nucleation (Bishnoi and Natarajan, 1996; Dai et al., 2014; Lee et al., 2013). In addition, several studies showed the link between induction time and the driving force applied to the system (temperature driving force or supercooling, pressure driving force and mass-transfer driving force) (Davies et al., 2009; Kashchiev and Firoozabadi, 2002; Liu et al., 2015; Natarajan et al., 1994; Skovborg et al., 1993). However, the effect of other factors related to the characteristics of the porous media, like water saturation, particle size, or the presence of a mesoporous space are still poorly understood.

3.1. Impact on amount of hydrates formed

3.1.1. Effect of water saturation

The influence of water saturation on the mass of gas hydrates formed was first investigated based on a set of experiments on silica sand with various water saturation conditions and particle size. Table 3 summarizes the experimental conditions applied to this set of experiments and the final water to hydrate conversion (based on the fixed hydration number of CO_2 hydrate). Water content is defined as the mass of water by the mass of solid particles (sand grains or Silica gel particles) initially introduced in the cell.

Table 3: CO_2 hydrate formation and dissociation results in a sandy matrix for several water saturations and particle size

Run	Sample state*	Particle size (µm)	Water mass (g)	Water saturation (%)	Mass of Solid particles (g)	Water content	Mass of hydrates formed (g)	Water conversion to hydrate (%)
1	F	Non-sieved sand	5.78	33.4	59.58	0.10	3.17	41.2
2	F		9.00	52.0	59.57	0.15	3.39	28.1
3	F		11.05	59.9	56.60	0.19	3.20	21.8
4	F		11.32	63.7	58.37	0.19	1.87	12.5
5	M		11.32	63.7	58.37	0.19	2.27	14.9
6	F		13.10	75.2	59.31	0.22	2.16	12.3
7	F		17.45	100	59.36	0.29	No hydrate formation succeeded	
8	F	PS01	10.34	53.4	54.16	0.19	4.47	32.3
9	F	PS02	9.37	51.5	57.15	0.16	3.60	28.7
10	F	PS03	9.20	51.8	58.36	0.16	3.16	25.7

*F: fresh sample. M: memory sample. In the latter state. Run 5 represents a repeatability test for Run 4 (without changing the sample).

The influence of water saturation on the amount of hydrates formed is also represented in Figure 7, with the mass of the hydrate formed and the rate of water to hydrate conversion as a function of water saturation of non-sieved silica sand. It is interesting to note that the amount of hydrates formed is not significantly different for water saturations ranging from 33 to 60 %. However, for higher water saturation (63 % and higher), the results show lower values of the mass of hydrates formed. It is also interesting to note that the rates of water conversion to hydrates are between 12 and 41 % and follow a decreasing tendency with the increase of water saturation. This is due to the fact that in the measurement cell the formation of hydrates takes place in a closed system after CO_2 injection. In fact, the gas first dissolves in water under temperature conditions outside the hydrate stability zone. After reaching a stable saturation, which corresponds to the same (*P*, *T*) conditions for all experiments, the system is closed. Thus, knowing that the density of CO_2 in vapor phase is higher than the density of CO_2 dissolved in liquid phase, the total amount of CO_2 in the system also decreases when increasing water saturation (and so decreasing the volume of the vapor phase). After closing the system, the temperature is decreased to form hydrates. With less CO_2 available in the system, and more water, then less hydrate is formed, as confirmed by the results from a previous solid fraction model based on an equilibrium balance on CO_2 in its different vapor, dissolved in liquid and hydrate phases (Marinhas et al., 2007). It is interesting to note that these mass balance results are in the same range of values as the present results from the calorimetric approach as seen in Figure 7 with the open and full green diamonds.

Another aspect that must be taken into consideration when investigating the effect of water saturation on gas hydrate formation is the spatial distribution of water in the porous volume. Under high water saturation conditions, the distribution of liquid and vapor phases limits the interfacial contact, and sometimes leads to the formation of hydrate plugs. This can prevent

428 the gas from accessing certain water zones in the pores. On the other hand, at low water
429 saturation, gas diffusion through the porous medium is facilitated due to a relatively larger
430 void volume.

431 For experiment 7 where silica sand is completely saturated with water (S_w = 100 %), the DTA
432 peak of hydrate formation was not detected and no pressure drop was observed despite a
433 relatively long experiment time (52 h). Indeed, the desired experimental pressure (2.5 MPa)
434 could not be reached within a reasonable time. This result suggests that with completely
435 saturated porous media, liquid-gas contact area through which CO_2 diffuses in water is
436 reduced. In addition, given that water occupies the total pore volume, the amount of CO_2
437 initially injected to reach the same experimental pressure conditions is reduced. Consequently,
438 hydrate formation is hindered.

439 Overall, these findings confirm the existence of a strong correlation between water saturation
440 and the amount of CO_2 hydrate formed, as it is reported in previous studies for CH_4 hydrates
441 in several porous media (Babu et al., 2013; Bagherzadeh et al., 2011; Ge et al., 2019; Kumar
442 et al., 2015; Pan et al., 2018). As the focus of this study is to appreciate optimal water
443 saturation conditions for an efficient cold storage system, the results demonstrate that a 50-
444 60 % water saturated system could be a suitable level to maximize the amount of energy
445 stored. This optimal saturation value is slightly lower than the value usually used in the
446 literature to improve hydrate formation kinetics around 70 % (Ge et al., 2019; Mekala et al.,
447 2014). However, further investigations should be carried out to study additional water
448 saturations. Moreover, a semi-batch configuration where CO_2 is continuously injected during
449 hydrate formation should be tested. Indeed, this gas-excess configuration could increase the
450 amount of hydrate formed and potentially the water to hydrate conversion rate. These results
451 also suggested that hydrate conversion rate could be influenced by the spatial distribution of

water in the pore volume. The latter is strongly related to the geometric characteristic of the porous media, which will be discussed in the following section.

3.1.2. Effect of particle size

For the study of the effect of particle size on CO_2 hydrate formation and dissociation in porous media, Fontainebleau Silica sand was sieved into 3 particle size classes: PS01, PS02 and PS03. Figure 8 shows the evolution of the formed hydrate mass and water to hydrate conversion rates as a function of the particle size classes for a given water saturation around 52.2 % corresponding to runs 8 to 10 in Table 3. The pore volume for the particle size classes being the same, the same quantity of water is used in the various sand samples. A clear decreasing tendency of the amount of hydrate mass and hydrate conversion rate as a function of the four particle size classes is observed. This pattern is due to the decrease of the specific area resulting from the increase of particle size. Indeed, for a larger specific area (smaller particle size) water is adsorbed on a larger surface area. This could potentially enhance the liquid-gas contact area, which can improve gas hydrate formation. This suggests that CO_2 hydrate formation occurs preferentially at the solid-liquid interfaces of sand particles. It is important to note that the mass of hydrates obtained within the non-sieved sand is close to the amount within PS02 because this class represents 80 % of the non-sieved sand**Erreur ! Source du renvoi introuvable.**. Alternatively, it is possible to assume that the fraction leftover representing 10 % has no significant influence on the hydrate conversion rate.

These findings are consistent with some previous studies reported in the literature (Bhattacharjee et al., 2015; Ge et al., 2019; Mekala et al., 2014; Qin et al., 2022) and mentioned in the introduction section. However, other studies demonstrated an opposite result (Adeyemo et al., 2010; Kumar et al., 2015; Lu et al., 2011; Pan et al., 2018). In this case, it has been suggested, globally, that hydrates formed in smaller pores may obstruct gas diffusion in the porous media. In their recent review Qin et al. (2021) also reported this inconsistency

between previous studies on the influence of particle size on hydrate formation. Indeed, the authors suggested that this discrepancy in the results of the above-mentioned studies might be due to the influence of other factors, such as the initial water saturation used in each study, the composition of the gas phase, the specific surface area, or even the experimental system and hydrate formation procedure used. Overall, further studies are needed, especially for CO_2 hydrates, considering the above-mentioned cross-factor effect to better understand the mechanisms involved in order to determine the influence of particle size on gas hydrates formation.

3.1.3. Effect of the morphology

In this section, results from the investigation of CO_2 hydrate formation and dissociation in two morphologically different porous media, silica sand and silica gel, are reported. Fontainebleau silica sand is considered as a uniform grain size structure (with only external porosity) and silica gel as a dual porosity media (with internal and external porosity). The data of mass hydrate formed and water to hydrate conversion rates are illustrated in Table 4. They are presented for dual porous silica gel with two distinct pore size and compared with the results obtained in Fontainebleau silica sand (detailed properties in the experimental section, Table 1).

For silica gel samples, three configurations of water saturation were tested:

1) Amount of water injected lower than the internal pore volume $V_w < V_p$ (Run 1 and 2)
2) Amount of water injected corresponding to the internal pore volume $V_w = V_p$ (Run 3, 4 and 6)
3) Amount of water injected greater than the pore volume $V_w > V_p$ (Run 5, 7 and 8); in this case, it is assumed that the water occupies the entire internal pore volume, but also a fraction of the interstitial space (external pore).

501 The water saturation of the internal pore volume of silica gel and of the interstitial space

502 are respectively denoted Sw_p and Sw_i.

503

Table 4: CO_2 hydrate formation and dissociation results in silica gel

Run	Pore size (nm)	Mass of water injected (g)	Water saturation of Pore volume Sw_p (%)	Water saturation of Interstitial space Sw_i (%)	Mass of solid particles (g)	Water content	Induction time (min)	Mass of hydrate formed (g)	Water to hydrate conversion rate (%)
1	100	5.93	53	0	15.99	0.37	No hydrate		
2		9.01	78	0	16.46	0.55	165	4.63	38.4
3		11.35	100	0	16.22	0.70	203	4.70	30.9
4		11.01	100	0	15.73	0.70	102	4.83	32.8
5		17.98	100	32	16.00	1.12	82	2.68	11.1
6	30	14.10	100	0	16.42	0.86	100	4.52	24.0
7		19.47	100	30	16.17	1.20	740	5.02	19.3
8		21.83	100	43	16.00	1.36	253	2.45	8.4

First, a comparison of hydrate formation and dissociation DTA signals obtained in both silica sand and silica gel with close initial water mass is illustrated in Figure 9 (for clarity, DTA peaks are overlapped). It should be noted that the DTA signal is a differential measurement between the two cells, and as mentioned earlier in this paper, the reference cell contains the same porous media as in the measurement cell for each experiment. Therefore, it can reasonably perform a comparative analysis of the DTA peaks without considering the difference in thermal conductivities of the two porous media (silica sand and silica gel). From Figure 9, it is interesting to notice higher and larger exothermic and endothermic DTA signal peaks for the experiments performed in silica gel compared to silica sand. This measurement indicates a significant difference in thermal behavior between the test cell and the reference cell in the case of silica gel compared to silica sand, thus, a greater amount of thermal energy stored/released in the silica gel media compared to silica sand. These results suggest a strong effect of the structural organization (morphology and water distribution) of the porous media on heat transfer in the system. Moreover, DTA signals for the majority of experiments performed in silica gel did not show a smaller second formation peak, except for one

experiment in 100 nm pore size silica gel (Run 3, 4). Whereas, all the experiments carried out in silica sand showed a multiple nucleation phenomenon expressed by the presence of a second DTA signal peak of very small intensity. It could be conceivably hypothesized that this difference may be related to the shape of the particles. Indeed, silica gel particles have a spherical shape compared to sand particles, which have rather irregular shapes. In the latter, the morphology of the void space could be more heterogeneous compared to a silica gel porous media. Thus, mass transfer could be affected by this heterogeneity, which can lead to multiple nucleation loci at delayed times. The amount of hydrate formed under several water saturation conditions of silica gel, and in the two distinct pore sizes, was then examined. The results of hydrate mass formed and water to hydrate conversion rates are shown in Table 4 and Figure 10. Globally, it can be seen from Figure 10 that the hydrate mass in silica gel, as well as water to hydrate conversion rates, are higher in comparison with silica sand. However, this difference is not in the same order of magnitude as DTA signal peaks shown in Figure 9. This is due to ice calibration (used to calculate the mass of hydrates formed) which is different, depending on the system configuration. In addition, the results indicate that a configuration of the system where water occupies only the pore volume of silica gel, water content lower than 1, seems to be a good option to enhance the amount of hydrate formed. This can be explained by the presence of a mesoporous volume in silica gel, which seems to enhance gas and water contact. Indeed, water can be adsorbed at the surface of silica gel inside the pores thanks to capillary forces, which leaves the interstitial space free for a better diffusion of gas through the porous media. Regarding water to hydrate conversion rate, the results show a decreasing tendency when the initial amount of water increase in the system. As it is observed in silica sand, when the amount of water in silica gel increases, it results in a decrease in the amount of CO_2 initially injected in the measurement cell of the DTA apparatus. Furthermore, when the water content is higher than 1 in silica gel, that means the

water amount is sufficient to saturate not only the pore volume but also the interstitial space, the system configuration is closed to that obtained in silica sand and the amount of hydrate formed are comparable in some cases. In this case, the formation of the hydrate could be affected by the heterogeneous distribution of water and gas in the porous media. This can explain the decrease in the amount of hydrate formed observed with both pore size of silica gel (100 nm and 30 nm).

3.2. Impact on induction time

3.2.1. Effect of water saturation

The influence of water saturation on induction time was first investigated based on a set of experiments on silica sand with various water saturation conditions and particle size. Table 5 summarizes the experimental conditions applied to this set of experiments.

Table 5: Induction time of CO_2 hydrate formation and dissociation results in a sandy matrix

Run	Particle size	Water saturation (%)	Induction time (min)	Driving force (% mol CO_2/mol H_2O)
1	Non-sieved sand	33.4	68	0.59
2		52.0	51	0.67
3		59.9	120	0.84
4		63.7	83	0.73
5		63.7	399	0.72
6		75.2	81	0.71
7		100	No hydrate formation succeeded -	
8	PS01	53.4	87	0.86
9	PS02	51.5	83	0.83
10	PS03	51.8	92	0.85

Figure 11a shows the induction time values obtained as a function of water saturation of the porous sample in the cell. To our knowledge, induction time data for CO_2 hydrates as a function of water saturation of the porous media are poorly known. Some authors provided induction time data for CO_2 hydrate formation in different porous media but at a unique water saturation (Rehman et al., 2022; Sahu et al., 2022) and these data are added to figure 11a for comparison. The induction time values are scattered and vary between 51 and 120 min for the

majority of the experiments except for Sahu et al. (2022). They showed an important induction time of 2083.8 min within a silica sand of 0.15 mm particle diameter at 70 % water saturation. The induction time dispersion may be due to several key factors such as the configuration of the experimental system (reactor type and design, the internal volume, operating conditions, driving force…). There are therefore biases of interpretation when different works are compared. A slight increase of induction time can be observed when water saturation of silica sand increases. However, for the repeated experiment at 63.7 % water saturation (Run 5, 5) (For this experiment, the sample was left about 210 min at 285 K before restarting the cooling process), it can be noted a considerable difference in the induction time compared to the rest of the experiments. This discrepancy in induction time may be related to a heterogeneous redistribution of the water within the porous media after hydrate dissociation. Indeed, the CO_2 hydrate formation experiments in this study are performed for an experimental temperature of 271.15 K and under pressure conditions around 2.5 MPa. Figure 11b shows the results of induction time as a function of the driving force. The latter is calculated using the method reported by Boufares et al. (2018). This method consists of estimating the CO_2 concentration in the liquid phase at Hydrate-Liquid-Vapor Equilibrium pressure corresponding to the experimental temperature (the super-saturation). It is interesting to note from Figure 11b that a slight increase of the driving force does not have a significant influence on induction time. The latter increases slightly but remains in a narrow range.

Overall, these results show that water saturation has small effect on induction time. The discrepancies observed may also be due to the stochastic nature of hydrate nucleation. However, given that these findings are based on a limited number of experiences, this analysis should thus be treated with considerable caution.

3.2.2. Effect of particle size

According to literature, pore size is one of the main parameters determining hydrate formation kinetic in porous media (Borchardt et al., 2016; Nguyen et al., 2020). The results in Table 5 showed that the induction time values at which CO_2 hydrate formation is detected for the 3-particle size classes are relatively homogeneous with an average value of 87±5 min. They present a difference of 35±5 min compared to the induction time obtained for non-sieved silica sand as shown on Figure 11b. Overall, it is difficult to establish from these results an obvious correlation between induction time and particle size of silica sand. The results reported in the literature seem to diverge regarding the effect of particle size on induction time. As observed by Qin et al. (2021), some studies demonstrated a positive effect of small particle size on shortening the induction time (Heeschen et al., 2016; Zhang et al., 2018). This may be due to a larger nucleation area when decreasing particle size. However, other studies found an opposite effect even though a similar particle size and porous media were used (Liu et al., 2015; Qin et al., 2021). Qin et al. (2021) suggested that the reason for this divergence is related to the fact that induction time is strongly affected by many other factors like: (1) the experimental method used to form hydrate, (2) the geometry of the experimental device, (3) the type of hydrate formed, etc. This could also explain the results obtained in this study.

3.2.3. Effect of the morphology

In this section, results related to the investigation of induction time according to different operating conditions: pore size, water saturation of silica gel pore volume and interstitial space and driving force were reported in Table 6.

Table 6: Operating conditions and results obtained from the experiments of CO2 hydrate formation and dissociation in silica gel

Run	Pore size (nm)	Mass of water injected (g)	Water saturation of Pore volume	Water saturation of Interstitial space S_{wi}	Induction time (min)	Driving force (% mol CO_2/mol H_2O)

			S_{wp} (%)	(%)		
1	100	5.93	53	0	No hydrate	
2		9.01	78	0	165	0.50
3		11.35	100	0	203	0.80
4		11.01	100	0	102	0.89
5		17.98	100	32	82	0.77
6	30	14.10	100	0	100	0.77
7		19.47	100	30	740	0.92
8		21.83	100	43	253	0.78

It is well known that the driving force, necessary to initiate the formation of hydrates in silica gels, increases when the pore sizes decrease because the thermodynamic equilibrium conditions are more difficult to reach. Therefore, at constant driving force, when the pore sizes decrease the induction time must increase. This can be seen in Figure 11b where for a driving force around 0.8 %mol CO_2/molH_2O, the induction time increases up to 25 % in 30 nm silica gels compared to 100 nm. Figure 12 gathers the result obtained for silica gel and silica sand as a function of the initial water content introduced in the porous media. It can be seen that induction time values for the experiments performed in silica gel are quite scattered between 82 and 235 min. A significant difference in the induction times was noted in the case of silica gel with an internal pore size of 30 nm, and a water saturation of the pore volume and the interstitial space (Run 7, ≈740 min). In addition, it can notice that for a similar initial water content, the induction time values obtained for silica gel are close, and slightly higher in some cases, than those obtained in Fontainebleau silica sand. For high water content, particularly in the case of 30 nm pore (Run 7 and 8) size silica gel, the induction time values are higher than in the case of low water content (Run 6). Knowing that for these two particular experiments, water occupies both the pore volume and the interstitial space, this points to the hypothesis that water-gas contact is hindered by the presence of water in the interstitial space.

627 Consequently, it is difficult to draw conclusions, given that hydrate nucleation is a stochastic
628 process. Furthermore, when water saturates partially the pore volume (S_{wp} = 53 %) which
629 corresponds to an initial water content of 0.37 (correspond to an initial water mass of 6 g)
630 (Run 1), gas hydrate formation was not detected (no DTA signal related to hydrate formation,
631 and no pressure and temperature variation). This may be due to the adsorption of water on the
632 internal pore surface of silica gel, which makes the amount of free water not sufficient for
633 hydrate formation.

634 ## 4. Conclusion

635 In an effort to provide new insights on the influence of key factors related to the use of porous
636 media on CO_2 hydrates formation and dissociation processes, with a differential thermal
637 analysis (DTA) approach, the effect of water saturation, particle size and the morphology of
638 the porous media on induction time, storage capacity and equilibrium conditions on the solid
639 mass fraction formed and the induction time was investigated:

640 • First, water distribution in a silica sand sample was investigated using X-ray micro-
641 tomography. The analysis of two volume portions taken from the total volume of the
642 30 %-water saturated silica sand sample allows us to reasonably state that the sample
643 preparation method used in this study provides a rather homogeneous distribution of
644 water over the total sample volume.
645 • For water saturation, the analysis of the results obtained with silica sand did not reveal
646 a noteworthy effect on the induction time. Furthermore, when water saturation
647 increases in a closed system and for the same initial pressure condition, the amount of
648 CO_2 initially injected in the cell decreases, which results in a lower mass of hydrates
649 formed, and thus, a lower water to hydrate conversion rates.
650 • For particle size, within silica sand, it has shown that this factor does not influence the
651 induction time, whereas, the results indicated a strong effect on the amount of hydrate

formed. Indeed, for a smaller particle size, liquid-gas contact area is enhanced due to water adsorption on a larger surface area. This can potentially enhance the amount of hydrate formed.

- Finally, this study investigated the influence of the morphology of the porous medium on hydrate formation and dissociation by using silica sand and spherical dual porous silica gel. Overall, the results showed a higher amount of thermal energy stored by hydrates formed in silica gel compared to Fontainebleau silica sand. Moreover, a configuration where water occupies only the pore volume of silica gel was found to be optimal. In addition, an inhibiting effect on the thermodynamic condition of hydrate stability was observed. It is well known in the literature that this effect becomes much more significant as pore size of silica gel particles decreases.

These results showed relatively clear correlations between the factors studied and the fraction of hydrates formed. However, the influence of these factors on the induction time is not obvious. This may be due to coupling problems between these different factors, but also to the lack of information on other factors such as wettability, which would deserve to be studied in depth. Due to the complexity of the characterization of gas hydrates induction time and the stochastic nature of hydrate nucleation, this study also requires a detailed statistical analysis with several replicate experiments. Overall, these findings add to a growing body of literature on the link between hydrate formation and dissociation process and the key factors related to the porous media. Despite this, the calorimetry work carried out in this study could be the basis for further sets of experiments in order to clearly identify optimal conditions for energy efficient CO_2 hydrate-based technologies such as cold storage systems.

CRediT authorship contribution statement

Fatima Doria Benmesbah: Methodology, Software, Investigation, Data curation, Writing – original draft, Visualization. **Pascal Clain:** Supervision, Validation, Visualization, Writing -

review & editing. **Olivia Fandino:** Supervision. **Veronique Osswald:** Validation, Visualization. **Laurence Fournaison:** Supervision, **Christophe Dicharry:** Resources, Methodology, Writing - review & editing. **Livio Ruffine:** Project administration, Resources, Supervision, Validation, Writing - review & editing. **Anthony Delahaye:** Project administration, Supervision, Validation, Visualization, Writing - review & editing.

Declaration of Competing Interest

The authors declare that they have no known competing financial interests or personal relationships that could have appeared to influence the work reported in this paper.

Acknowledgment

The authors would like to thank Fatou-Toutie Ndoye and Graciela Alvarez Leguizamo, researchers at Université Paris-Saclay, FRISE, INRAE, for their technical support, advice and guidance with the X-ray microtomography device. We are also grateful to Elyamin Dahmana, for his direct technical help on CO_2 hydrates formation and dissociation experiments using the DTA device. The authors also acknowledge anonymous reviewers for their valuable suggestions and remarks.

5. References

Adeyemo, A., 2008. Post combustion capture of carbon dioxide through hydrate formation in silica gel column.

Adeyemo, A., Kumar, R., Linga, P., Ripmeester, J., Englezos, P., 2010. Capture of carbon dioxide from flue or fuel gas mixtures by clathrate crystallization in a silica gel column. International Journal of Greenhouse Gas Control 4, 478-485.

Akbari, H., Mertol, A., 1989. Thermal Energy Storage for Cooling of Commercial Buildings, in: Kılkışş, B., Kakaç, S. (Eds.), Energy Storage Systems. Springer Netherlands, Dordrecht, pp. 315–347.

Anderson, G.K., 2003. Enthalpy of dissociation and hydration number of carbon dioxide hydrate from the Clapeyron equation. The Journal of Chemical Thermodynamics 35, 1171-1183.

Babu, P., Kumar, R., Linga, P., 2013. Medium pressure hydrate based gas separation (HBGS) process for pre-combustion capture of carbon dioxide employing a novel fixed bed reactor. International Journal of Greenhouse Gas Control 17, 206-214.

Bagherzadeh, S.A., Moudrakovski, I.L., Ripmeester, J.A., Englezos, P., 2011. Magnetic Resonance Imaging of Gas Hydrate Formation in a Bed of Silica Sand Particles. Energy & Fuels 25, 3083-3092.

Bhattacharjee, G., Kumar, A., Sakpal, T., Kumar, R., 2015. Carbon Dioxide Sequestration: Influence of Porous Media on Hydrate Formation Kinetics. ACS Sustainable Chemistry & Engineering 3, 1205-1214.
Bishnoi, P.R., Natarajan, V., 1996. Formation and decomposition of gas hydrates. Fluid Phase Equilibria 117, 168-177.
Borchardt, L., Nickel, W., Casco, M., Senkovska, I., Bon, V., Wallacher, D., Grimm, N., Krause, S., Silvestre-Albero, J., 2016. Illuminating solid gas storage in confined spaces – methane hydrate formation in porous model carbons. Physical Chemistry Chemical Physics 18, 20607-20614.
Boufares, A., Provost, E., Dalmazzone, D., Osswald, V., Clain, P., Delahaye, A., Fournaison, L., 2018. Kinetic study of CO2 hydrates crystallization: Characterization using FTIR/ATR spectroscopy and contribution modeling of equilibrium/non-equilibrium phase-behavior. Chemical Engineering Science 192, 371-379.
Chami, N., Bendjenni, S., Clain, P., Osswald, V., Delahaye, A., Fournaison, L., Dalmazzone, D., 2021. Thermodynamic characterization of mixed gas hydrates in the presence of cyclopentane as guest molecule for an application in secondary refrigeration. Chemical Engineering Science 244, 116790.
Cheng, C., Wang, F., Tian, Y., Wu, X., Zheng, J., Zhang, J., Li, L., Yang, P., Zhao, J., 2020. Review and prospects of hydrate cold storage technology. Renewable and Sustainable Energy Reviews 117, 109492.
Chong, Z.R., Yang, M., Khoo, B.C., Linga, P., 2016. Size Effect of Porous Media on Methane Hydrate Formation and Dissociation in an Excess Gas Environment. Industrial & Engineering Chemistry Research 55, 7981-7991.
Clain, P., 2014. Couplage entre le stockage et distribution de froid par coulis d'hydrates. Sorbonne Université, Paris.
Dai, S., Lee, J.Y., Santamarina, J.C., 2014. Hydrate nucleation in quiescent and dynamic conditions. Fluid Phase Equilibria 378, 107-112.
Darbouret, M., Cournil, M., Herri, J.-M., 2005. Rheological study of TBAB hydrate slurries as secondary two-phase refrigerants. International Journal of Refrigeration 28, 663-671.
Davies, S.R., Hester, K.C., Lachance, J.W., Koh, C.A., Dendy Sloan, E., 2009. Studies of hydrate nucleation with high pressure differential scanning calorimetry. Chemical Engineering Science 64, 370-375.
Delahaye, A., Fournaison, L., Dalmazzone, D., 2018. Use of Hydrates for Cold Storage and Distribution in Refrigeration and Air-Conditioning Applications, Gas Hydrates 2. John Wiley & Sons, Ltd, pp. 315-358.
Delahaye, A., Fournaison, L., Marinhas, S., Martínez, M.C., 2008. Rheological study of CO2 hydrate slurry in a dynamic loop applied to secondary refrigeration. Chemical Engineering Science 63, 3551-3559.
Dicharry, C., Duchateau, C., Asbaï, H., Broseta, D., Torré, J.-P., 2013. Carbon dioxide gas hydrate crystallization in porous silica gel particles partially saturated with a surfactant solution. Chemical Engineering Science 98, 88-97.
Dufour, T., Hoang, H.M., Oignet, J., Osswald, V., Clain, P., Fournaison, L., Delahaye, A., 2017. Impact of pressure on the dynamic behavior of CO2 hydrate slurry in a stirred tank reactor applied to cold thermal energy storage. Applied Energy 204, 641-652.
Englezos, P., 1993. Clathrate hydrates. Industrial & Engineering Chemistry Research 32, 1251-1274.
Englezos, P., Kalogerakis, N., Dholabhai, P.D., Bishnoi, P.R., 1987. Kinetics of formation of methane and ethane gas hydrates. Chemical Engineering Science 42, 2647-2658.
Fitzgerald, G.C., Castaldi, M.J., Schicks, J.M., 2014. Methane Hydrate Formation and Thermal Based Dissociation Behavior in Silica Glass Bead Porous Media. Industrial & Engineering Chemistry Research 53, 6840-6854.
Fournaison, L., Delahaye, A., Chatti, I., Petitet, J.-P., 2004. CO2 Hydrates in Refrigeration Processes. Industrial & Engineering Chemistry Research 43, 6521-6526.
Ge, B.-B., Zhong, D.-L., Lu, Y.-Y., 2019. Influence of water saturation and particle size on methane hydrate formation and dissociation in a fixed bed of silica sand. Energy Procedia 158, 5402-5407.

760 Gupta, A., Lachance, J., Sloan, E.D., Koh, C.A., 2008. Measurements of methane hydrate heat of
761 dissociation using high pressure differential scanning calorimetry. Chemical Engineering Science 63,
762 5848-5853.
763 Handa, Y.P., Stupin, D.Y., 1992. Thermodynamic properties and dissociation characteristics of
764 methane and propane hydrates in 70-.ANG.-radius silica gel pores. The Journal of Physical Chemistry
765 96, 8599-8603.
766 Hasnain, S.M., 1998. Review on sustainable thermal energy storage technologies, Part II: cool
767 thermal storage. Energy Conversion and Management 39, 1139-1153.
768 Heeschen, K.U., Schicks, J.M., Oeltzschner, G., 2016. The promoting effect of natural sand on
769 methane hydrate formation: Grain sizes and mineral composition. Fuel 181, 139-147.
770 Jerbi, S., Delahaye, A., Fournaison, L., Haberschill, P., 2010. Characterization of CO2 hydrate
771 formation and dissociation kinetics in a flow loop. International Journal of Refrigeration 33, 1625-
772 1631.
773 Joshi, A., Sangwai, J.S., Das, K., Sami, N.A., 2013. Experimental investigations on the phase
774 equilibrium of semiclathrate hydrates of carbon dioxide in TBAB with small amount of surfactant.
775 International Journal of Energy and Environmental Engineering 4, 11.
776 Kang, S.-P., Lee, H., Ryu, B.J., 2001. Enthalpies of dissociation of clathrate hydrates of carbon dioxide,
777 nitrogen, (carbon dioxide + nitrogen), and (carbon dioxide + nitrogen + tetrahydrofuran). The Journal
778 of Chemical Thermodynamics 33, 513-521.
779 Kang, S.-P., Lee, J.-W., Ryu, H.-J., 2008. Phase behavior of methane and carbon dioxide hydrates in
780 meso- and macro-sized porous media. Fluid Phase Equilibria 274, 68-72.
781 Kang, S.-P., Lee, J., Seo, Y., 2013. Pre-combustion capture of CO2 by gas hydrate formation in silica
782 gel pore structure. Chemical Engineering Journal 218, 126-132.
783 Kashchiev, D., Firoozabadi, A., 2002. Nucleation of gas hydrates. Journal of Crystal Growth 243, 476-
784 489.
785 Kumar, A., Khatri, D., Lee, J.D., Kumar, R., 2016. Crystallization kinetics for carbon dioxide gas hydrate
786 in fixed bed and stirred tank reactor. Korean Journal of Chemical Engineering 33, 1922-1930.
787 Kumar, A., Sakpal, T., Linga, P., Kumar, R., 2013. Influence of contact medium and surfactants on
788 carbon dioxide clathrate hydrate kinetics. Fuel 105, 664-671.
789 Kumar, A., Sakpal, T., Roy, S., Kumar, R., 2015. Methane hydrate formation in a test sediment of sand
790 and clay at various levels of water saturation. Canadian Journal of Chemistry 93, 874-881.
791 Laugier, F., Andriantsiferana, C., Wilhelm, A.M., Delmas, H., 2008. Ultrasound in gas–liquid systems:
792 Effects on solubility and mass transfer. Ultrasonics Sonochemistry 15, 965-972.
793 Lee, K., Lee, S.-H., Lee, W., 2013. Stochastic nature of carbon dioxide hydrate induction times in Na-
794 montmorillonite and marine sediment suspensions. International Journal of Greenhouse Gas Control
795 14, 15-24.
796 Li, G., Hwang, Y., Radermacher, R., 2012. Review of cold storage materials for air conditioning
797 application. International Journal of Refrigeration 35, 2053-2077.
798 Lievois, J.S., Perkins, R., Martin, R.J., Kobayashi, R., 1990. Development of an automated, high
799 pressure heat flux calorimeter and its application to measure the heat of dissociation and hydrate
800 numbers of methane hydrate. Fluid Phase Equilibria 59, 73-97.
801 Lin, W., Dalmazzone, D., Fürst, W., Delahaye, A., Fournaison, L., Clain, P., 2014. Thermodynamic
802 properties of semiclathrate hydrates formed from the TBAB+TBPB+water and
803 CO2+TBAB+TBPB+water systems. Fluid Phase Equilibria 372, 63-68.
804 Linga, P., Clarke, M.A., 2017. A Review of Reactor Designs and Materials Employed for Increasing the
805 Rate of Gas Hydrate Formation. Energy & Fuels 31, 1-13.
806 Linga, P., Daraboina, N., Ripmeester, J.A., Englezos, P., 2012. Enhanced rate of gas hydrate formation
807 in a fixed bed column filled with sand compared to a stirred vessel. Chemical Engineering Science 68,
808 617-623.
809 Linga, P., Haligva, C., Nam, S.C., Ripmeester, J.A., Englezos, P., 2009. Gas Hydrate Formation in a
810 Variable Volume Bed of Silica Sand Particles. Energy & Fuels 23, 5496-5507.

Linga, P., Kumar, R., Lee, J.D., Ripmeester, J., Englezos, P., 2010. A new apparatus to enhance the rate of gas hydrate formation: Application to capture of carbon dioxide. International Journal of Greenhouse Gas Control 4, 630-637.
Liu, W., Wang, S., Yang, M., Song, Y., Wang, S., Zhao, J., 2015. Investigation of the induction time for THF hydrate formation in porous media. Journal of Natural Gas Science and Engineering 24, 357-364.
Loveday, J.S., Nelmes, R.J., 2008. High-pressure gas hydrates. Phys. Chem. Chem. Phys. 10, 937-950.
Lu, H., Kawasaki, T., Ukita, T., Moudrakovski, I., Fujii, T., Noguchi, S., Shimada, T., Nakamizu, M., Ripmeester, J., Ratcliffe, C., 2011. Particle size effect on the saturation of methane hydrate in sediments – Constrained from experimental results. Marine and Petroleum Geology 28, 1801-1805.
Malagar, B.R.C., Lijith, K.P., Singh, D.N., 2019. Formation & dissociation of methane gas hydrates in sediments: A critical review. Journal of Natural Gas Science and Engineering 65, 168-184.
Marinhas, S., Delahaye, A., Fournaison, L., 2007. Solid fraction modelling for CO2 and CO2–THF hydrate slurries used as secondary refrigerants. International Journal of Refrigeration 30, 758-766.
Martínez, M.C., Dalmazzone, D., Fürst, W., Delahaye, A., Fournaison, L., 2008. Thermodynamic properties of THF + CO2 hydrates in relation with refrigeration applications. AIChE Journal 54, 1088-1095.
Mekala, P., Busch, M., Mech, D., Patel, R.S., Sangwai, J.S., 2014. Effect of silica sand size on the formation kinetics of CO2 hydrate in porous media in the presence of pure water and seawater relevant for CO2 sequestration. Journal of Petroleum Science and Engineering 122, 1-9.
Natarajan, V., Bishnoi, P.R., Kalogerakis, N., 1994. Induction phenomena in gas hydrate nucleation. Chemical Engineering Science 49, 2075-2087.
Nguyen, N.N., Galib, M., Nguyen, A.V., 2020. Critical Review on Gas Hydrate Formation at Solid Surfaces and in Confined Spaces—Why and How Does Interfacial Regime Matter? Energy & Fuels 34, 6751-6760.
Oya, S., Aifaa, M., Ohmura, R., 2017. Formation, growth and sintering of CO2 hydrate crystals in liquid water with continuous CO2 supply: Implication for subsurface CO2 sequestration. International Journal of Greenhouse Gas Control 63, 386-391.
Pan, Z., Liu, Z., Zhang, Z., Shang, L., Ma, S., 2018. Effect of silica sand size and saturation on methane hydrate formation in the presence of SDS. Journal of Natural Gas Science and Engineering 56, 266-280.
Park, J., Seo, Y.-T., Lee, J.-w., Lee, H., 2006. Spectroscopic analysis of carbon dioxide and nitrogen mixed gas hydrates in silica gel for CO2 separation. Catalysis Today 115, 279-282.
Prah, B., Yun, R., 2018. CO2 hydrate slurry transportation in carbon capture and storage. Applied Thermal Engineering 128, 653-661.
Qin, Y., Bao, R., Shang, L., Zhou, L., Meng, L., Zang, C., Sun, X., 2022. Effects of Particle Size and Types of Porous Media on the Formation and Occurrence of Methane Hydrate in Complex Systems. Energy & Fuels 36, 655-668.
Qin, Y., Pan, Z., Liu, Z., Shang, L., Zhou, L., 2021. Influence of the Particle Size of Porous Media on the Formation of Natural Gas Hydrate: A Review. Energy & Fuels 35, 11640-11664.
Rehman, A.N., Lal, B., Pendyala, R., Yusoff, M.H.M., 2022. Unusual CO2 hydrate formation in porous media: Implications on geo-CO2 storage laboratory testing methods. Materials Today: Proceedings 57, 1363-1368.
Sahu, C., Sircar, A., Sangwai, J.S., Kumar, R., 2022. Effect of sodium tripolyphosphate (STPP) and tetrasodium pyrophosphate (TSPP) on the formation kinetics of CO2 hydrate in bulk and porous media in the presence of pure water and seawater relevant for CO2 sequestration. International Journal of Greenhouse Gas Control 114, 103564.
Shindo, Y., Lund, P.C., Fujioka, Y., Komiyama, H., 1993. Kinetics and mechanism of the formation of CO2 hydrate. International Journal of Chemical Kinetics 25, 777-782.
Skovborg, P., Ng, H.J., Rasmussen, P., Mohn, U., 1993. Measurement of induction times for the formation of methane and ethane gas hydrates. Chemical Engineering Science 48, 445-453.
Sloan, E.D., 1998. Physical/chemical properties of gas hydrates and application to world margin stability and climatic change. Geological Society, London, Special Publications 137, 31–50.

Sloan, E.D., Fleyfel, F., 1992. Hydrate dissociation enthalpy and guest size. Fluid Phase Equilibria 76, 123-140.
Sloan, E.D., Koh, C.A., 2007. Clathrate Hydrates of Natural Gases, 3rd edition ed. CRC Press, Boca Raton.
Smith, D.H., Wilder, J.W., Seshadri, K., 2002. Thermodynamics of Carbon Dioxide Hydrate Formation in Media with Broad Pore-Size Distributions. Environmental Science & Technology 36, 5192-5198.
Torré, J.-P., Dicharry, C., Ricaurte, M., Daniel-David, D., Broseta, D., 2011. CO2 capture by hydrate formation in quiescent conditions: In search of efficient kinetic additives. Energy Procedia 4, 621-628.
Turner, D.J., Cherry, R.S., Sloan, E.D., 2005. Sensitivity of methane hydrate phase equilibria to sediment pore size. Fluid Phase Equilibria 228-229, 505-510.
Uchida, T., Ebinuma, T., Takeya, S., Nagao, J., Narita, H., 2002. Effects of Pore Sizes on Dissociation Temperatures and Pressures of Methane, Carbon Dioxide, and Propane Hydrates in Porous Media. The Journal of Physical Chemistry B 106, 820-826.
Wang, J., Zhang, L., Ge, K., Dong, H., 2021. Capillary pressure in the anisotropy of sediments with hydrate formation. Fuel 289, 119938.
Wang, X., Dennis, M., 2017. Thermal energy harvest in the discharge of CO2 semi-clathrate hydrate in an emulated cold storage system. Applied Thermal Engineering 124, 725-733.
Wang, X., Dennis, M., Hou, L., 2014. Clathrate hydrate technology for cold storage in air conditioning systems. Renewable and Sustainable Energy Reviews 36, 34-51.
Wang, X., Zhang, F., Lipiński, W., 2020. Carbon dioxide hydrates for cold thermal energy storage: A review. Solar Energy 211, 11-30.
Wang, Z., Li, F., Fan, T., Xiong, W., Yang, B., 2015. Research on the Application of Gas Hydrate in Cool Storage Air Conditioning. Procedia Engineering 121, 1118-1125.
Yang, M., Song, Y., Jiang, L., Liu, Y., Wang, X., 2015. Behaviour of hydrate-based technology for H2/CO2 separation in glass beads. Separation and Purification Technology 141, 170-178.
Yang, M., Song, Y., Ruan, X., Liu, Y., Zhao, J., Li, Q., 2012. Characteristics of CO2 Hydrate Formation and Dissociation in Glass Beads and Silica Gel. Energies 5, 925-937.
Zhang, B., Zhou, L., Liu, C., Zhang, Q., Wu, Q., Wu, Q., Liu, C., 2018. Influence of sediment media with different particle sizes on the nucleation of gas hydrate. Natural Gas Industry B 5, 652-659.
Zhang, F., Wang, X., Wang, B., Lou, X., Lipiński, W., 2022. Effects of silica gel nanopores and surfactants on CO2 hydrate formation kinetics—An experimental and modeling study. Chemical Engineering Science 262, 118002.
Zhang, X., Li, J., Wu, Q., Wang, C., Nan, J., 2015. Experimental study on the effect of pore size on carbon dioxide hydrate formation and storage in porous media. Journal of Natural Gas Science and Engineering 25, 297-302.
Zhang, Y., Li, X.-S., Chen, Z.-Y., Li, G., Wang, Y., 2016. Effects of particle and pore sizes on the formation behaviors of methane hydrate in porous silica gels. Journal of Natural Gas Science and Engineering 35, 1463-1471.
Zhang, Y., Li, X., Chen, Z., Xia, Z., Wang, Y., Li, G., 2017. Formation Behavior and Controlling Factor of Methane Hydrate in Porous Media. Energy Procedia 142, 4044-4049.

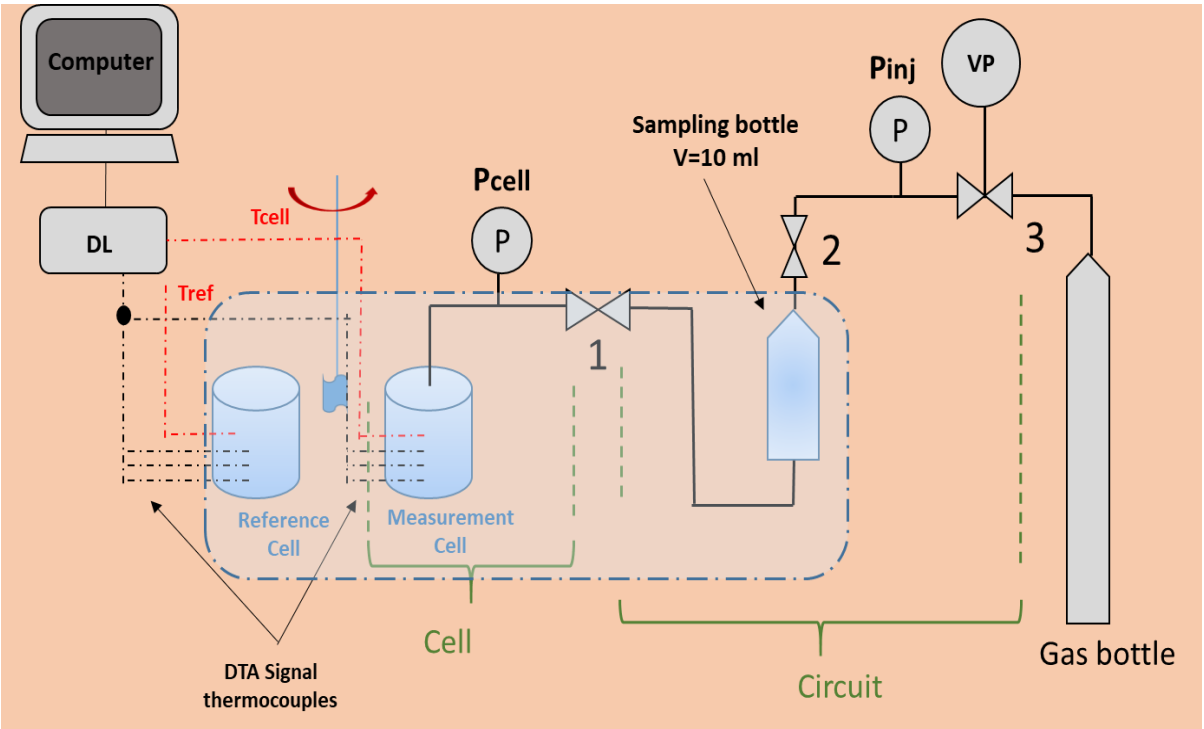

Figure 1: Schematic diagram of the DTA experimental apparatus. (DL) Data logger, (P) Pressure transducer, (T_{cell}, T_{ref}) Thermocouple to measure direct temperature, (VP) Vacuum pump, the blue area corresponds to a temperature-controlled bath in which the two cells are immersed, as well as the sampling cylinder

905

906

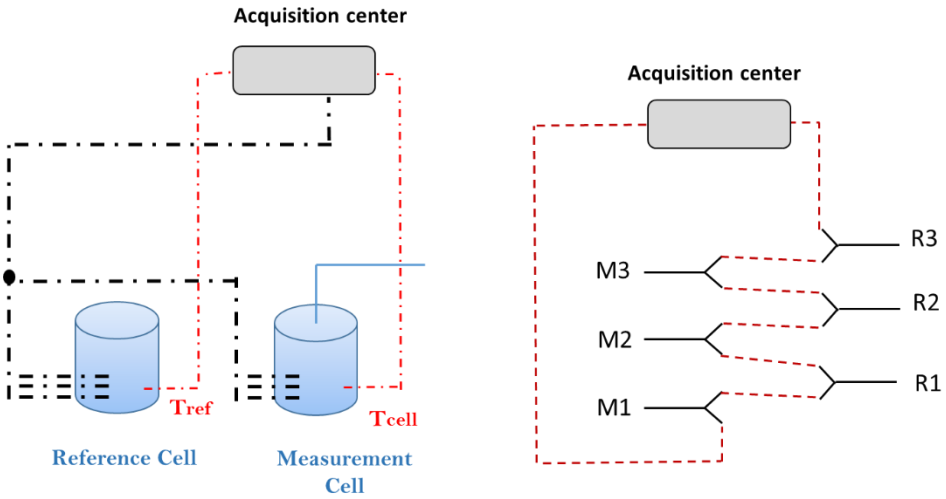

907

908 Figure 2: Diagram of the six thermocouples connected in series to obtain the DTA signal. M1,
909 M2 and M3 correspond to the thermocouples placed in the measuring cell. R1, R2 and R3
910 correspond to the thermocouples placed in the reference cell

911

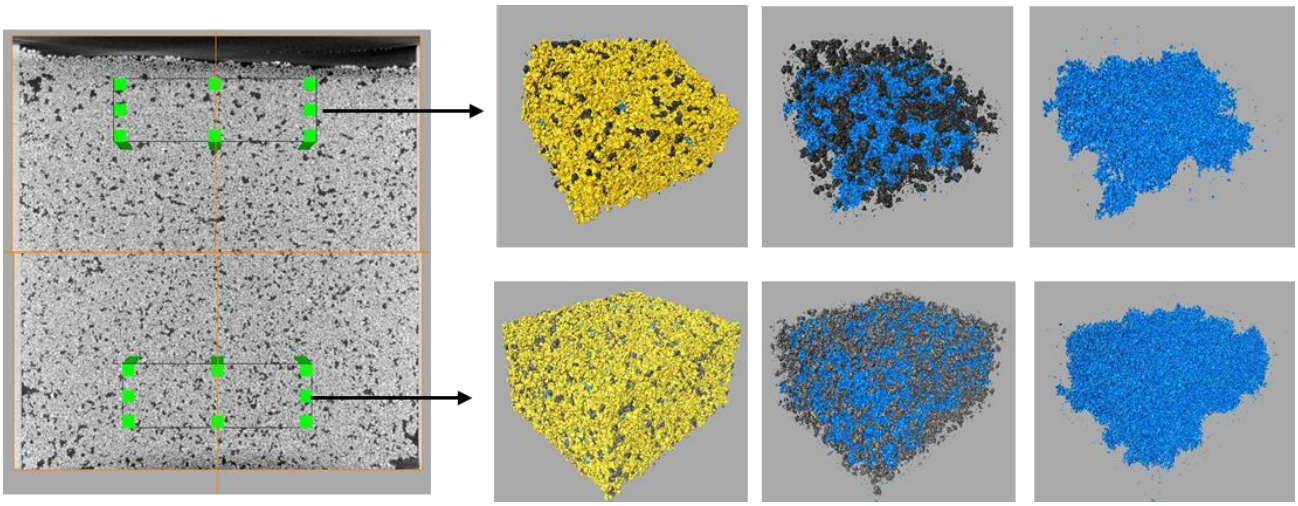

Figure 3: CT scan analysis of a sand sample for a water saturation of 66%. Sand is represented in yellow, water in blue and air in dark grey.

912

913

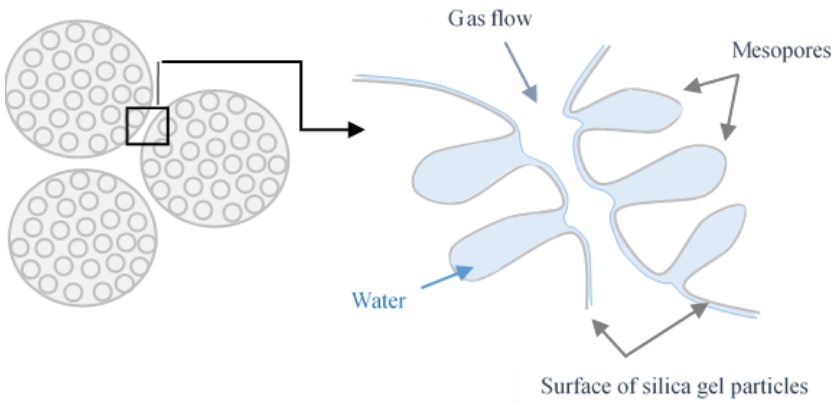

914 Figure 4: Schematic illustration of water occupying the mesoporous volume of silica gel
915 particles

916

a)

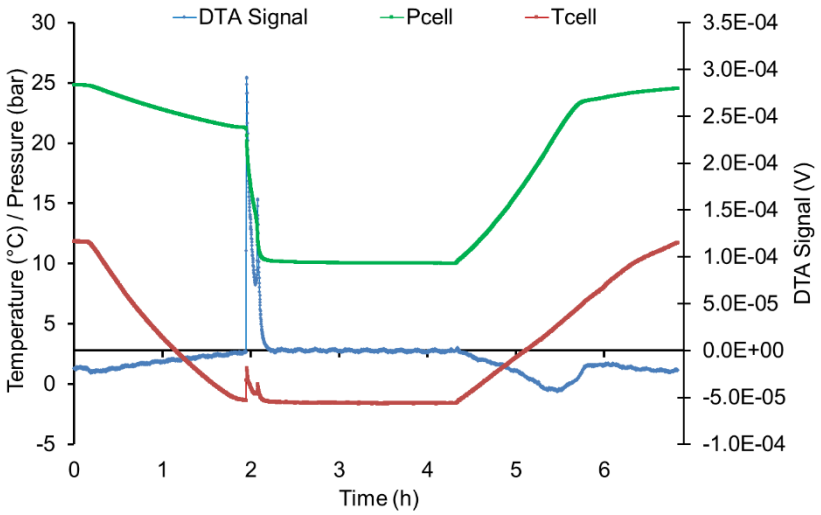

b)

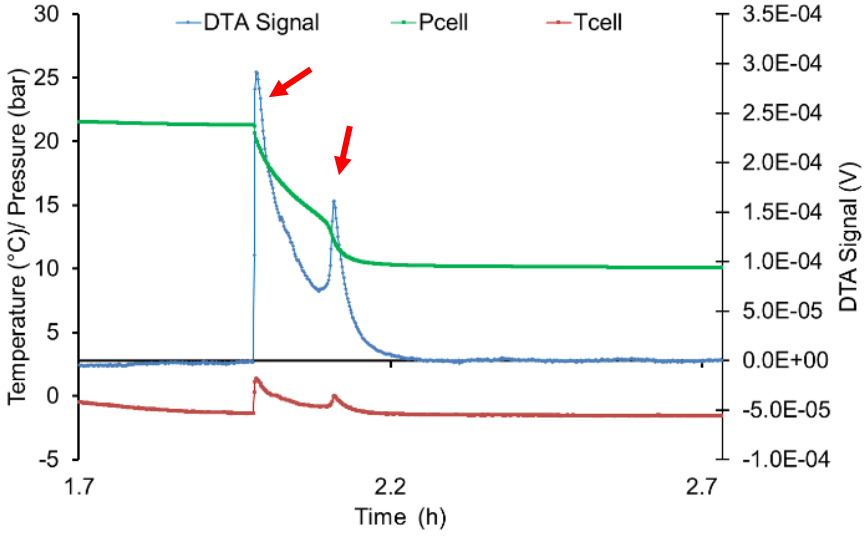

c)

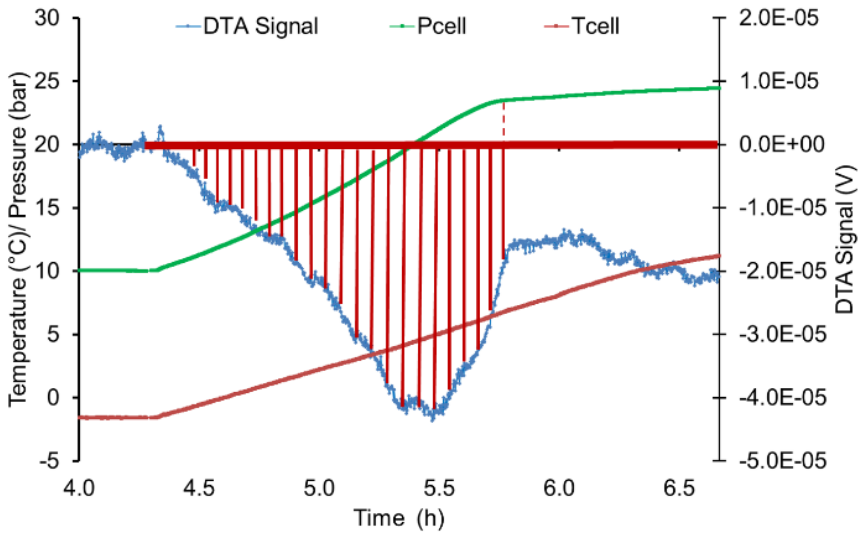

Figure 5: a) Temperature, pressure and DTA signal profiles during CO_2 hydrate formation and dissociation in silica sand at 33 % water

saturation. Figures b) and c) focus on CO_2 hydrates formation peak and CO_2 hydrates dissociation peak respectively.

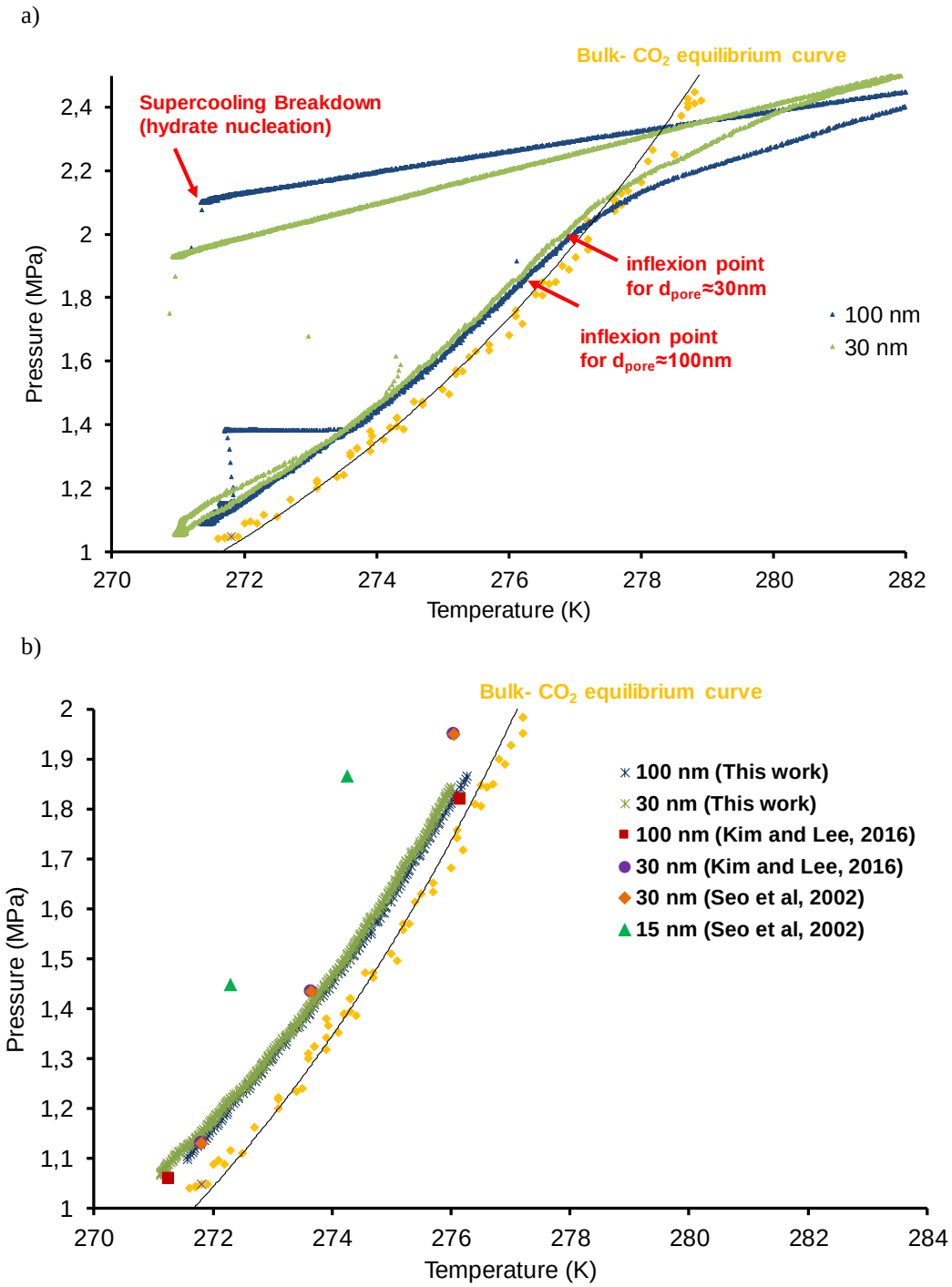

Figure 6: Temperature vs pressure profile of CO_2 gas hydrates in silica gel with several pore sizes. Results of previous studies in the literature are also reported (Kim and Lee, 2016; Seo et al., 2002)

921

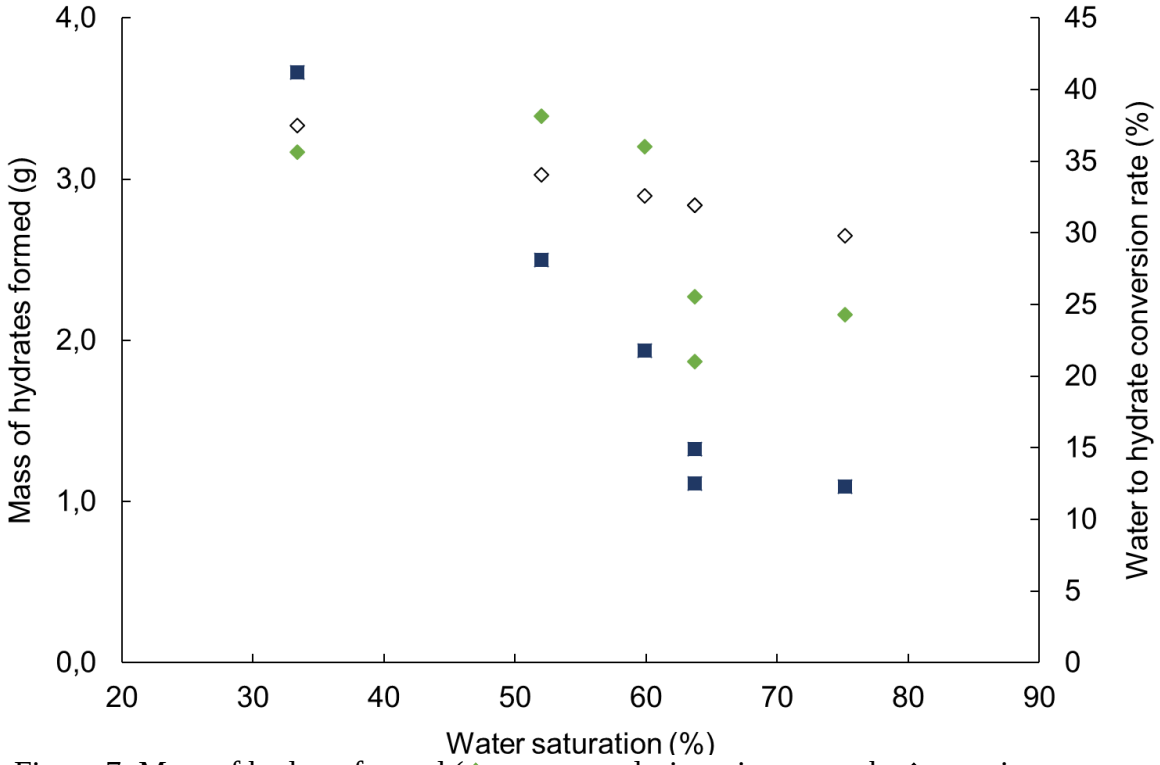

Figure 7: Mass of hydrate formed (◆: present calorimetric approach; ◇: previous mass balance approach (Marinhas et al., 2007) and water to hydrate conversion rate (■) as a function of water saturation of silica sand.

922

923

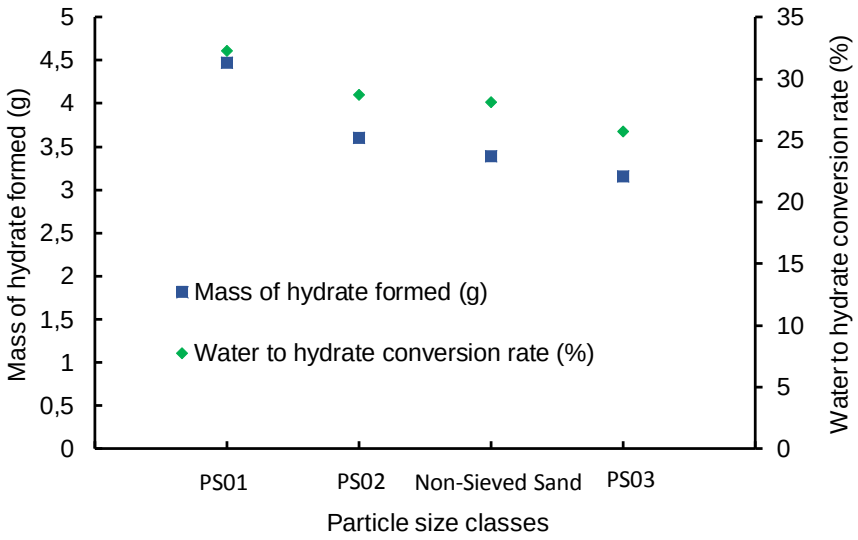

Figure 8: Mass of hydrate formed (◆) and water to hydrate conversion rate (■) as a function of particle size of silica sand.

924

925

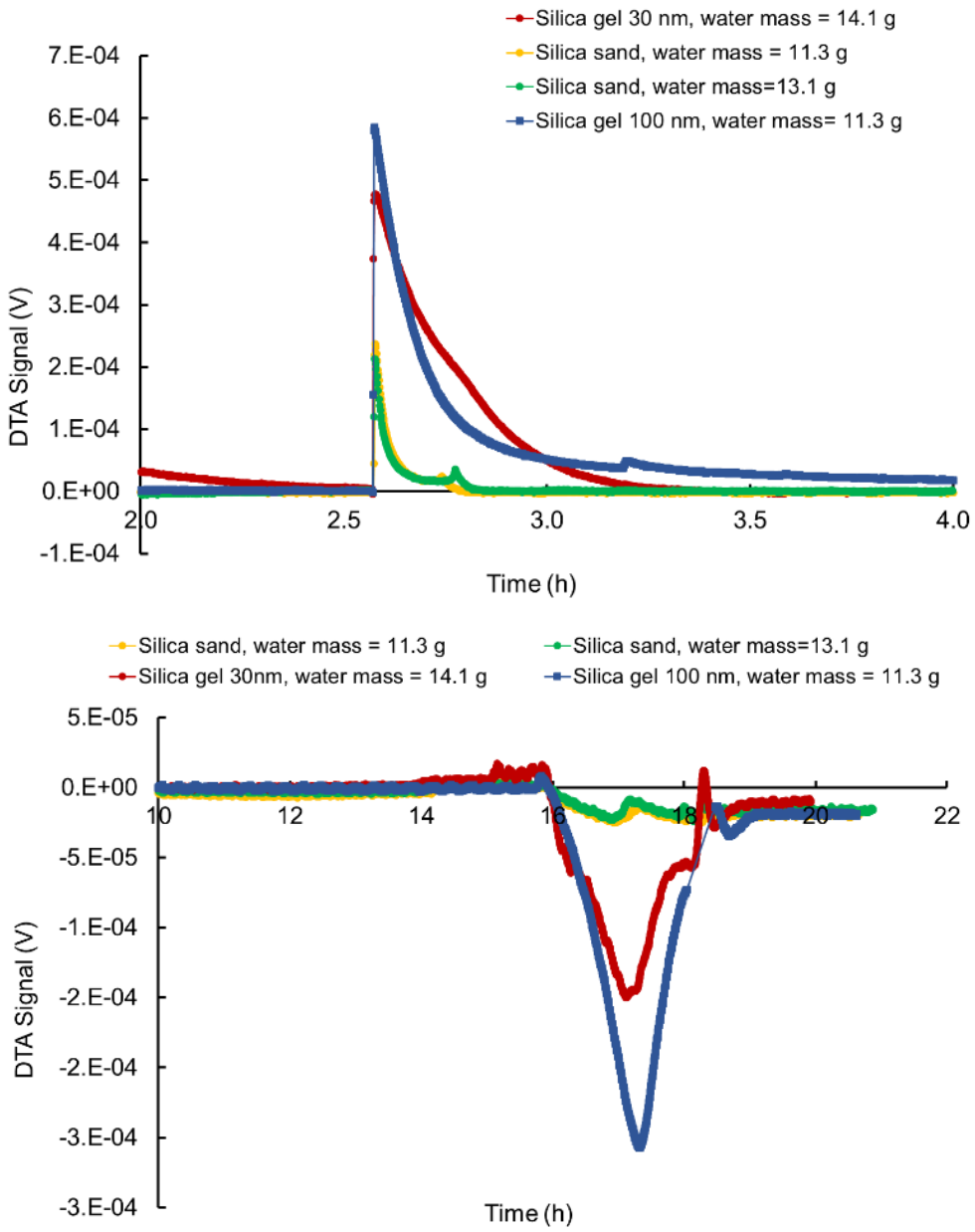

Figure 9: Comparison of DTA signal of CO_2 hydrate formation peaks in silica sand (Run 4 and 6, Table 3), and silica gel (Run 3 and 6, Table 5)

926

927

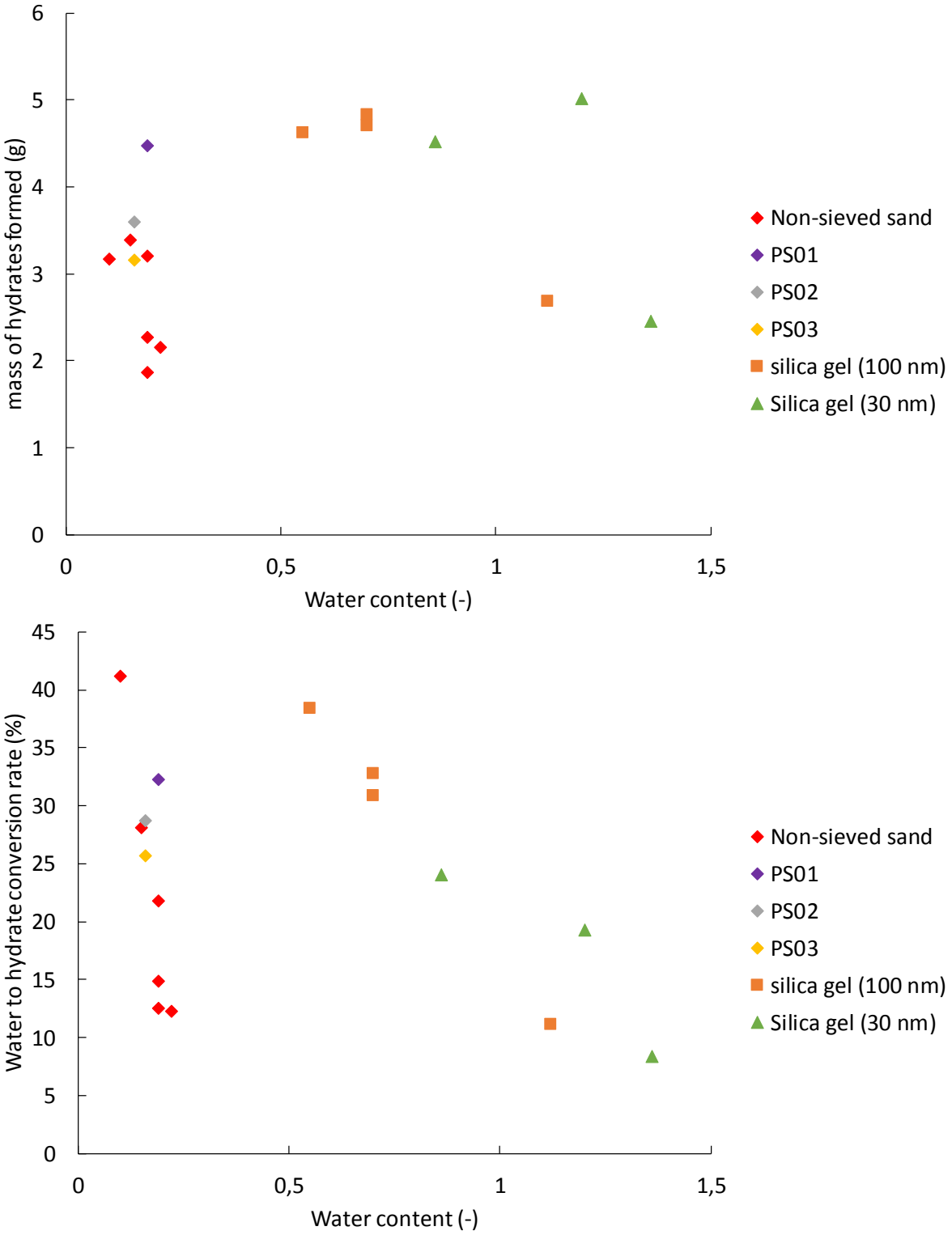

Figure 10: Mass of hydrate formed and water to hydrate conversion rate as a function of initial water content.

928

929

930

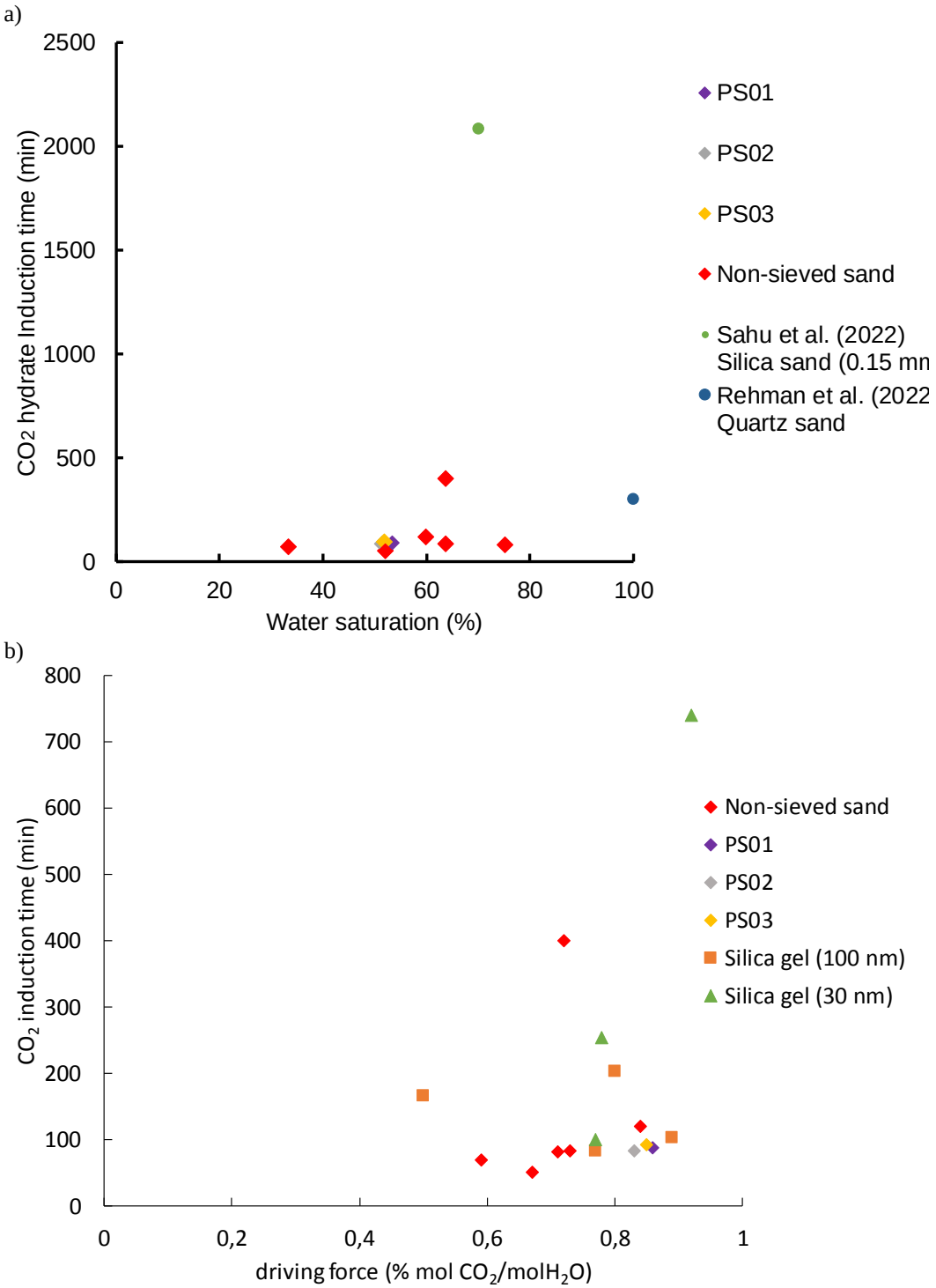

Figure 11: Induction time as a function of a) water saturation of silica sand and particles size, b) the driving force induced by the experimental conditions.

931

932

933

934

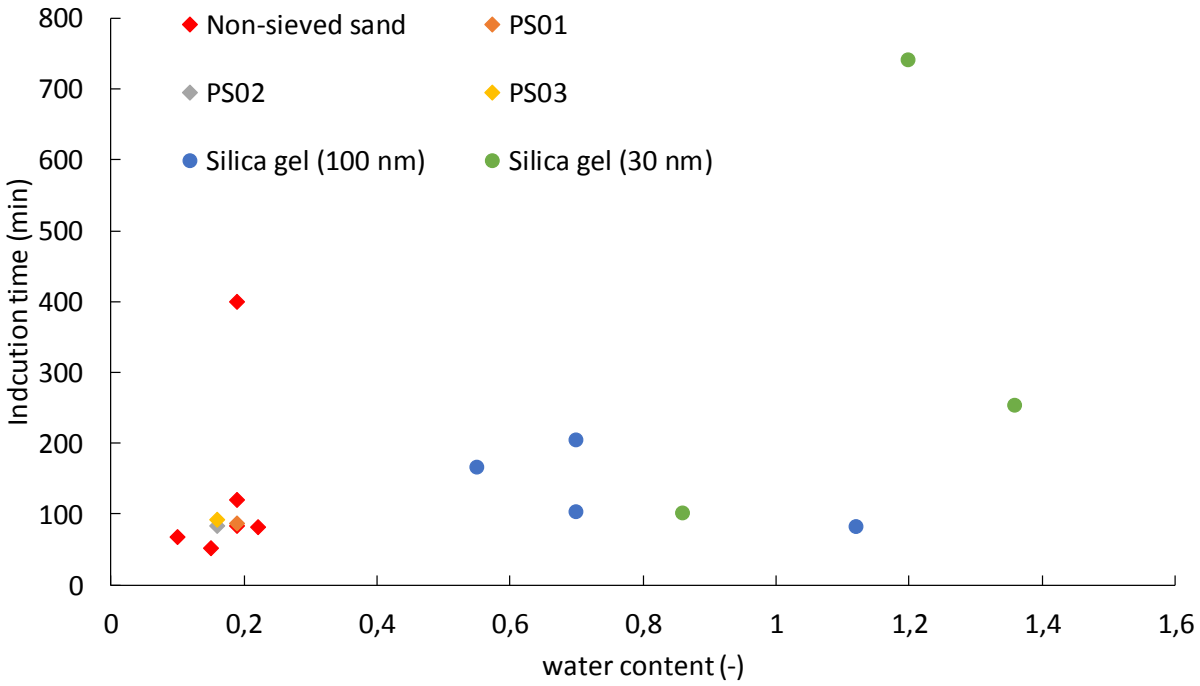

Figure 12: Induction time in silica sand, 100 nm silica gel and 30 nm silica gel as a function of initial water content.

935

936

937